



## OPEN ACCESS

## EDITED BY

Anne-Sophie Bouvier,  
Université de Lausanne, Switzerland

## REVIEWED BY

Aurelie Germa,  
University of South Florida, United States  
Emma J. Liu,  
University College London,  
United Kingdom

## \*CORRESPONDENCE

Abigail Metcalfe,  
✉ abigail.metcalfe@uca.fr

## †PRESENT ADDRESS

Abigail Metcalfe,  
Laboratoire Magmas et Volcans, OPGC,  
Université Clermont Auvergne,  
Clermont-Ferrand, France  
Roberto Moretti,  
Università della Campania "Luigi  
Vanvitelli", Dipartimento di Ingegneria,  
Aversa, Italy

RECEIVED 12 January 2023

ACCEPTED 07 June 2023

PUBLISHED 23 June 2023

## CITATION

Metcalfe A, Moune S, Moretti R,  
Komorowski J-C and Aubry TJ (2023),  
Volatile emissions from past eruptions at  
La Soufrière de Guadeloupe (Lesser  
Antilles): insights into degassing  
processes and atmospheric impacts.  
*Front. Earth Sci.* 11:1143325.  
doi: 10.3389/feart.2023.1143325

## COPYRIGHT

© 2023 Metcalfe, Moune, Moretti,  
Komorowski and Aubry. This is an open-  
access article distributed under the terms  
of the [Creative Commons Attribution  
License \(CC BY\)](https://creativecommons.org/licenses/by/4.0/). The use, distribution or  
reproduction in other forums is  
permitted, provided the original author(s)  
and the copyright owner(s) are credited  
and that the original publication in this  
journal is cited, in accordance with  
accepted academic practice. No use,  
distribution or reproduction is permitted  
which does not comply with these terms.

# Volatile emissions from past eruptions at La Soufrière de Guadeloupe (Lesser Antilles): insights into degassing processes and atmospheric impacts

Abigail Metcalfe<sup>1\*†</sup>, Séverine Moune<sup>1,2,3</sup>, Roberto Moretti<sup>1,3†</sup>,  
Jean-Christophe Komorowski<sup>1</sup> and Thomas J. Aubry<sup>4</sup>

<sup>1</sup>Université Paris Cité, Institut de Physique Du Globe de Paris, CNRS UMR, Paris, France, <sup>2</sup>Laboratoire Magmas et Volcans, Observatoire de Physique du Globe de Clermont-Ferrand, Université Clermont Auvergne, Clermont-Ferrand, France, <sup>3</sup>Observatoire Volcanologique et Sismologique de Guadeloupe, Institut de Physique Du Globe de Paris, Gourbeyre, France, <sup>4</sup>Department of Earth and Environmental Sciences, University of Exeter, Penryn, United Kingdom

Volatiles exert a critical control on volcanic eruption style and in turn impact the near source environment and global climate. La Soufrière de Guadeloupe in the Lesser Antilles has been experiencing volcanic unrest since 1992, increasing to a peak in 2018. The lack of data available on volatiles from past eruptions, and the well-developed hydrothermal system makes understanding deep-released volatile behaviour challenging. In this study, we analyse new melt inclusions and shed light on the volatile lifecycle and impacts at La Soufrière de Guadeloupe. We focus on four eruptions: 1657 CE (Vulcanian), 1010 CE (Plinian), 341 CE (Strombolian) and 5680 BCE (Plinian), and compare to the well-studied 1530 CE (Sub-Plinian) eruption. The maximum volatile content of these eruption melt inclusions are: 4.42 wt% H<sub>2</sub>O, 1700 CO<sub>2</sub> ppm, 780 ppm S, 0.36 wt% Cl and 680 ppm F. We observe a decrease in S content over time indicating the whole system is evolving by early separation of FeS, resulting in a lower S content in younger magma. Using the CHOSETTO v1 model, we modelled degassing paths related to decompression at low pressures, suggesting the majority of S degassing has occurred during magma ascent. We also calculate the SO<sub>2</sub> emissions using the petrologic method, and while the 1657 CE, 1530 CE and 341 CE eruptions have negligible emissions (0.0001–0.001 Mt of SO<sub>2</sub>), the 1010 CE and 5680 BCE eruptions (0.2 Mt and 0.3 Mt of SO<sub>2</sub>, respectively) are greater. Using the SO<sub>2</sub> emissions and plume height, we calculated the climate forcing associated with each event. The 1010 CE and 5680 BCE Plinian eruptions produced a peak global mean stratospheric aerosol optical depth (SAOD) of 0.0055 and 0.0062, respectively. This suggests, that even the largest eruptions of La Soufrière de Guadeloupe did not exert a significant climate forcing individually, but are important contributors to the volcanic stratospheric sulfate aerosol background resulting from relatively moderate but frequent explosive eruptions. Overall, this study provides new insights into degassing processes and climate forcing not only at La Soufrière de Guadeloupe, but also for other basaltic-andesitic, magmatic-hydrothermal systems. These new constraints are vital particularly if the volcano is currently in a state of unrest and will contribute to improving monitoring crisis management and long-term planning.

## KEYWORDS

La Soufrière de Guadeloupe, volatile emissions, climate forcing, melt inclusions, degassing processes, atmospheric impacts

## 1 Introduction

Volatiles are the driving engine of volcanic phenomena; meaning the behaviour of volatiles are key in understanding volcanic processes. Volatiles are chemical constituents of a magma which are present in small amounts (on the order of a few weight percent) and partition preferably into a gas phase at low pressures (e.g., Edmonds and Wallace, 2017). The volatile phase is usually predominantly made up of H<sub>2</sub>O, CO<sub>2</sub>, sulphur and halogens (Cl and F) and plays a key role in eruptive dynamics. Indeed, volatiles control the growth, size, abundance and overpressure in bubbles, the growth and composition of crystal phases, magma differentiation, ascent and convection, as well as, on reaching the atmosphere, an impact on the environment and climate (e.g., Wilson et al., 1980; Sisson and Grove, 1993; Roggensack et al., 1997; Sparks et al., 1997; Wallace, 2005; Gurenko et al., 2005; Davidson and Kamenetsky, 2007; Kelley and Cottrell, 2009; Balcone-Boissard et al., 2010; Edmonds and Wallace, 2017; Marshall et al., 2022).

Volatiles can be derived from various depths or structural levels of the magma plumbing system according to where storage and degassing of magma is occurring (e.g., Scailliet and Pichavant, 2003). This is important to consider at arc volcanoes where magmatic processes are hypothesised to occur across a wide range of pressures. Volatiles can be present as both an exsolved, multicomponent vapour phase (if the magma is vapour saturated) or dissolved in the magma (if the magma is vapour undersaturated; e.g., Wallace, 2003). Vapour saturation occurs when the total partial pressure of dissolved volatiles in the magma is equal to the confining pressure (Edmonds and Wallace, 2017). Magmas, particularly intermediate to silicic magmas, become vapour saturated at low pressures due to cooling and crystallisation and underplating by CO<sub>2</sub>-rich magmas (e.g., Wallace, 2001; 2003; Edmonds and Wallace, 2017). Processes such as magma crystallisation can result in volatile oversaturation and subsequent exsolution and bubbles forming; this increases pressure in the magma reservoir and may trigger an eruption (e.g., Tait et al., 1989).

In addition to ash, during an eruption the injection of large quantities of volatiles can result in important impacts on the near source environment (e.g., Carlsen et al., 2021) and on global climate (e.g., Marshall et al., 2022). In particular, volcanic sulphur form volcanic sulphate aerosols which interact with Sun and Earth radiation and modulate Earth energy balance and climate (Robock, 2000). Stratospheric volcanic sulfate aerosols, formed from volcanic sulphur injected above the tropopause (ca. 9–16 km altitude depending on the latitude and season considered), have a lifetime of 1–3 years and spread globally (McCormick et al., 1995; Macdonald and Wordsworth, 2017). They backscatter solar radiation and result in a net surface cooling, for example, the 1991 Mount Pinatubo injected ca. 15 Mt of SO<sub>2</sub> at 25 km height (Guo et al., 2004) and resulted in a global-mean cooling of 0.5°C for a year (McCormick et al., 1995). Eruptions injecting on the order of 0.1–1 Mt of SO<sub>2</sub> into the stratosphere have much smaller climate impacts but are also much more frequent, and collectively they have a discernable

footprint on forcing and large-scale climate metrics such as global mean surface temperature (Solomon et al., 2011; Santer et al., 2014; Schmidt et al., 2018).

Volatiles also play an important role at volcanic systems during quiescent phases of activity, when they are passively degassed. Volatiles in the exsolved phase are thought to be transported through permeable bubble networks (Eichelberger et al., 1986), or through the magma mush along quasi-brittle fractures at high gas fractions and through viscous fingering which could allow relatively fast migration (Gonnermann and Manga, 2003; Edmonds and Herd, 2007; Cabrera et al., 2011; Huber et al., 2011; Castro et al., 2012; Oppenheimer et al., 2015). It is particularly important to consider mafic underplating of a more silicic magma, given the presence of an exsolved phase (Annen et al., 2006). Indeed, the presence of a volatile-saturated magma will favour the process of volatile exsolution which in turn will trigger heating and remobilization of the magma above (e.g., Bachmann and Bergantz, 2006). Crystal mushes are also thought to 'hold' exsolved gases in melt layers which in some cases, can contribute to rapid outgassing of volatiles (Huber et al., 2011; Oppenheimer et al., 2015).

La Soufrière de Guadeloupe (hereby referred to as La Soufrière) in the Lesser Antilles has been experiencing increasing unrest since 1992; the unrest reached a peak in 2018 when an earthquake was felt by the population (Moretti et al., 2020a). This volcano has a well-developed hydrothermal system in which deep gases re-equilibrate and mix with groundwaters (Brombach et al., 2000; Allard et al., 2014; Villemant et al., 2014; Tamburello et al., 2019; Moretti et al., 2020a; Moretti et al., 2020b; Moretti et al., 2021; Inostroza et al., 2022a; Inostroza et al., 2022b; Moune et al., 2022). The hydrothermal system screens the actual input of volatile components from the magma beneath and makes our understanding of magma behaviour at this system difficult. Indeed, hot magmatic gases infiltrating hydrothermal aquifers become partly depleted in their most water-soluble acid components (SO<sub>2</sub>, HCl, HF) because of cooling and scrubbing into deep circulating groundwater (Hedenquist and Lowenstern, 1994; Symonds et al., 2001; Moretti and Stefánsson, 2020). This leads to acid, relatively oxidized, and highly reactive solutions that neutralize by reacting with wall rocks and leaching cations which then boil. This liberates the geothermally re-equilibrated steam-dominated vapors enriched in CO<sub>2</sub>, H<sub>2</sub>S, H<sub>2</sub>, CH<sub>4</sub> and CO which feed surface fumaroles (Giggenbach, 1988; Giggenbach, 1997; Reed, 1997; Symonds et al., 2001; Moretti and Stefánsson, 2020). Given the ongoing unrest and the lack of data available on volatiles in past eruptions of La Soufrière, it is important to understand and track the release of volatiles in the magmatic system and their behaviour during eruptions. To make progress, this study provides new insights on the volatile life cycle at La Soufrière using melt inclusion data from five eruptions (1657 CE, 1530 CE, 1010 CE, 341 CE and 5680 BCE).

## 2 Geological and magmatic setting

Guadeloupe is composed of several islands and is in the central segment of the Lesser Antilles Arc. The Lesser Antilles were formed due to the subduction of the American plate under the Caribbean

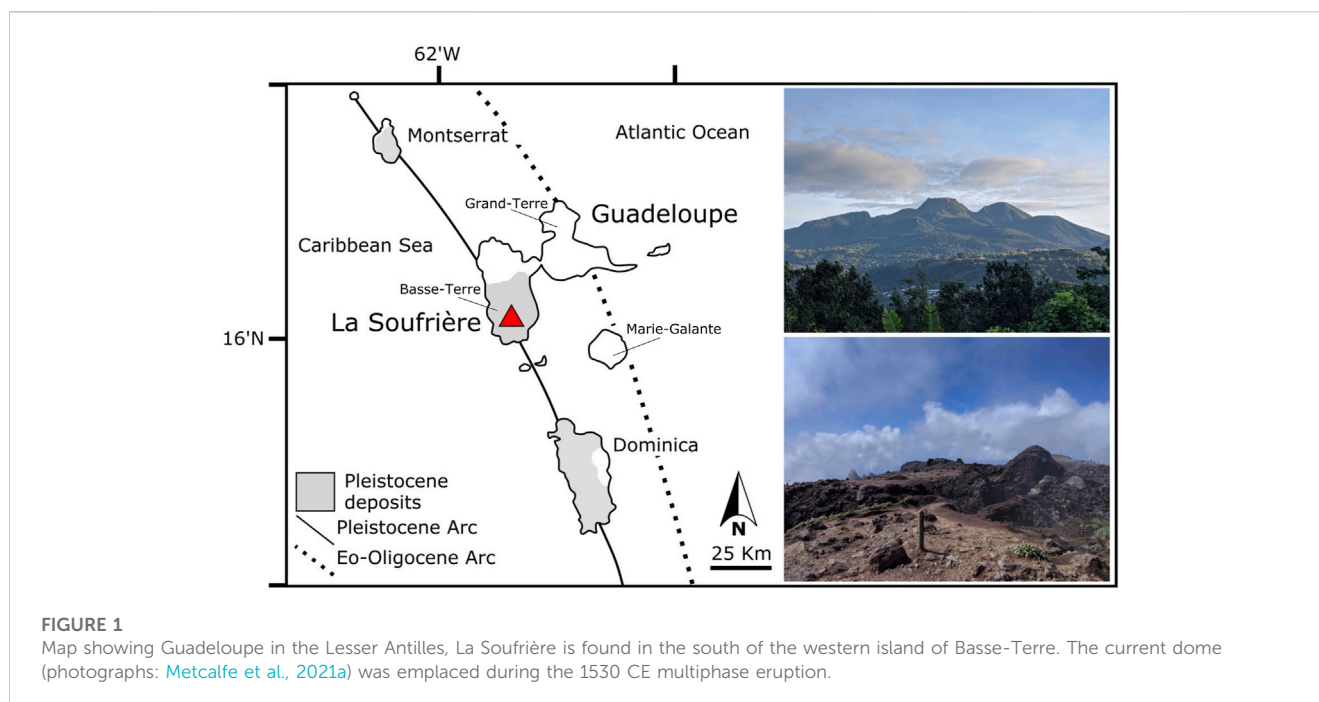


plate at a rate of  $\sim 1.9$  cm/yr (Macdonald and Holcombe, 1978; McCann and Sykes, 1984; Jarrard, 1986; Rosencrantz and Sclater, 1986; Deng and Sykes, 1995; Dixon et al., 1998; DeMets et al., 2000; Feuillet et al., 2011; Symithe et al., 2015). The eastern islands of Guadeloupe (Grand-Terre and Marie-Galante) are associated with the external arc, and the western island of Basse-Terre is associated with the active inner arc (ca. 2.8 Ma, Plio-Pleistocene; Macdonald et al., 2000; Komorowski et al., 2005; Boudon et al., 2008; Samper et al., 2007; Kopp et al., 2011; Figure 1).

Basse-Terre is composed of seven eruptive complexes with the Grande Découverte Soufriere complex (GDS) hosting the most recent volcanic activity observed in Guadeloupe, including La Soufrière, and occupies one-third of the island of Basse-Terre (Komorowski et al., 2005; Figure 1). La Soufrière is a basaltic-andesitic stratovolcano that was formed by a succession of lava flows, domes, pyroclastic sequences from explosive eruptions with sustained and collapsing plumes and explosive hydrothermal or activity. These deposits are intercalated between the debris avalanche deposits from a unique succession of at least nine partial edifice collapse events that occurred in the last 9,150 years (Komorowski et al., 2005; Boudon et al., 2007; Komorowski et al., 2008; Komorowski et al., 2013; Komorowski et al., 2022). On average eruption products in the GDS have whole rock compositions spanning a range of compositions from basaltic-andesite to andesite (Metcalfe et al., 2022). However, the scoria cones of Echelle and of La Citerne are mainly basaltic composition, despite a mixed basaltic and andesite bimodal lava flow in the central part of the Echelle scoria cone (Metcalfe et al., 2023).

Legendre (2012) and Komorowski et al. (2012, 2013) report numerous, previously unknown explosive eruptions of La Soufrière with the majority being multiphase eruptions. The plume heights reported are calculated from isopleth data reported in Komorowski

et al. (2008), Legendre (2012), Esposti Ongaro et al. (2020) and Komorowski et al. (2022), and are representative of the

Maximum plume heights above sea level (a.s.l.). Here, we provide a brief summary of the five La Soufrière eruptions discussed in this paper in order to contextualise the results and implications (Table 1). Detailed stratigraphy, radiocarbon dating, and eruptive deposit analysis available in Legendre (2012).

## 2.1 Relevant eruptive history of La Soufrière de Guadeloupe

### 2.1.1 The 5680 BCE eruption

The 5680 BCE (GDS15) eruption is the first and most violent magmatic eruption preserved in the geological record of the La Soufrière with an estimated VEI 4 (Volcanic Explosivity Index; Newhall and Self, 1982). This eruption generated a sustained eruption column reached a maximum height of 10–25 km a.s.l. and had a minimum estimated erupted volume of  $\sim 0.1$  km<sup>3</sup>, with scoria fallout found 7 km from the vent (Komorowski et al., 2012; Legendre, 2012; Komorowski et al., 2013).

### 2.1.2 The 341 CE eruption

The next eruption studied is the scoria cone eruption of Echelle, which is estimated to have occurred at 341 CE (GDS 6) (Boudon et al., 1988; Komorowski et al., 2005). This eruption occurred as magmatic activity migrated 0.8–1.4 km SE from the main La Soufrière vent, with the Echelle scoria cone erupted in a  $\sim N120$  structural alignment with La Soufrière (Feuillet et al., 2011). The Echelle eruption was a Strombolian-style eruption, interpreted as VEI 2 event, with a minimum erupted volume of 0.001 km<sup>3</sup> and an estimated 1–15 km a.s.l. eruption column (Legendre, 2012).

**TABLE 1** Summary table for the eruptions studied. \*from Pichavant et al., 2018 calculated by difference, all other volatile data is from SIMS and or EMPA measurements (Metcalfe et al., 2022). We report our standard deviations on the mean values of >10 analyses in brackets. Our analytical uncertainty on the volatile values is ±5%.

| Eruption | Event  | Vent         | VEI | Eruption style   | Volume erupted (km <sup>3</sup> ) | Eruption plume height (km) | Mean bulk comp. SiO <sub>2</sub> (wt%) | Mean MI SiO <sub>2</sub> (wt%) | Mean GM SiO <sub>2</sub> (wt%) | Volatile content |      |      |               |      |      |      |      |
|----------|--------|--------------|-----|--|-----------------------------------|----------------------------|--|--------------------------------|--------------------------------|------------------|------|------|---------------|------|------|------|------|
|          |        |              |     |  |                                   |                            |  |                                |                                | Max. MI (wt%)    |      |      | Mean GM (wt%) |      |      |      |      |
|          |        |              |     |  |                                   |                            |  | H <sub>2</sub> O               | CO <sub>2</sub>                | S                | Cl   | F    | S             | Cl   | F    |      |      |
| 1657 CE  | GDS 1  | La Soufrière | 2–3 | Vulcanian  | 0.001                             | 1–15                       | 58.1 (±2.0)                            | 71.3 (±1.9)                    | 62.8 (±2.9)                    | 4.14             | 0.07 | 0.06 | 0.36          | 0.05 | 0.01 | 0.24 | 0.01 |
| 1530 CE  | GDS 2  | La Soufrière | 3   | Sub-plinian, flank collapse, partial edifice collapse and lava dome growth | 0.09                              | 16–18                      | 57.5 (±1.6)                            | 73.7 (±1.9)                    | 71.2 (±3.3)                    | 5.6*             | -    | 0.05 | 0.35          | 0.02 | 0.02 | 0.16 | 0.02 |
| 1010CE   | GDS 3  | La Soufrière | 4   | Plinian with laterally directed blast and lave dome growth                 | 0.2                               | 10–25                      | 58 (±1.6)                              | 67.6 (±2.4)                    | 68.3 (±3.3)                    | 4.42             | 0.04 | 0.07 | 0.35          | 0.04 | 0.02 | 0.20 | 0.04 |
| 341 CE   | GDS 6  | Echelle      | 2   | Strombolian with monogenetic cone eruption                                 | 0.001                             | 1–15                       | 51.2 (±1.7)                            | 69.9 (±3.7)                    | 64.0 (±3.5)                    | -                | 0.2  | 0.02 | 0.33          | 0.05 | 0.02 | 0.02 | 0.04 |
| 5680 BCE | GDS 15 | La Soufrière | 4   | Plinian  | 0.2                               | 10–25                      | -                                      | 69.5 (±4.3)                    | 63.9 (±5.1)                    | 4.19             | 0.09 | 0.08 | 0.29          | 0.09 | 0.01 | 0.14 | 0.01 |

### 2.1.3 The 1010 CE eruption

The most recent Plinian eruption occurred at 1,010 ± 10 CE (GDS 3) and is categorised as VEI 4 explosive eruption. As with the 5680 BCE eruption the eruptive volume was estimated at ~0.1 km<sup>3</sup> and the eruptive column height estimated at 10–25 km a.s.l. Unlike the 5680 BCE eruption, the 1010 CE eruption was a multiphase eruption, also associated with a dome-building phase, which produced a laterally-directed explosion (blast) and high-energy pyroclastic density currents (Legendre, 2012).

### 2.1.4 The 1530 CE eruption

The most well-studied archetypal multiphase eruption of the La Soufrière episode is the 1530 CE eruption (GDS 2) which began with a partial edifice collapse followed by a phreatic explosive phase, a paroxysmal sub-Plinian explosive phase and that ended with emplacement of the current lava dome. This eruption is described in detail by Boudon et al. (2008); Komorowski et al. (2008); Komorowski et al. (2012); Komorowski et al. (2013); Pichavant et al. (2018); Esposti Ongaro et al. (2020). The eruption is categorised as VEI 3 with an estimated and revised eruptive volume of 0,07 to 0.09 km<sup>3</sup> (Legendre, 2012; Esposti Ongaro et al., 2020), the maximum plume height is constrained by Esposti Ongaro et al. (2020) at 16–18 km a.s.l., both based on extensive field analysis.

### 2.1.5 The 1657 CE eruption

Finally, we studied the most recent magmatic eruption which occurred in 1,657 ± 20 CE (GDS 1) (Komorowski et al., 2012; Legendre, 2012; Komorowski et al., 2013; Metcalfe et al., 2021a; Metcalfe et al., 2021b). This eruption was a small, explosive Vulcanian eruption (VEI 2–3), with a minimum estimated erupted volume of ~0.001 km<sup>3</sup> and an eruptive column height estimated at 1–15 km a.s.l., with no evidence for associated flank collapse or dome activity reported.

## 2.2 Recent activity at La Soufrière de Guadeloupe

Following the 1657 CE magmatic eruption, six phreatic/hydrothermal non-magmatic explosions have occurred (Feuillard et al., 1983; Komorowski et al., 2005; Hincks et al., 2014; Rosas-Carbajal et al., 2016). The most recent sequence of 26 phreatic explosions occurred during a phreatic eruption between July 1976 and March 1977. This changed the mechanical state of the dome through the opening of new major fractures and widening and deepening of existing fractures and craters and has had an important effect on the evolution of the system (Komorowski et al., 2005; Rosas-Carbajal et al., 2016; Moretti et al., 2020a). The period of minimal activity ended in May 1992 when seismic swarms and a new degassing phase began with summit fumarole reactivation (Zlotnicki et al., 1994; OVSG-IPGP, 1999; Komorowski et al., 2001; Komorowski et al., 2005).

Degassing has continued to evolve with new fumarolic vents appearing and pre-existing fumaroles reactivating (temperature range for these fumaroles: 96°C–110°C; Jessop et al., 2021), with locally high-velocity degassing. Between April 2017–December 2018 unrest reached a maximum and the highest level since

1976–1977 (Moretti et al., 2020a). Seismicity in particular was observed to reach a peak on 27 April 2018 when a M 4.1 earthquake, located approximately 3 km below the surface and 2.5 km NW of La Soufrière, was felt by the Basse-Terre population. This was the largest volcanic earthquake in 42 years (OVSG-IPGP, 1999; Moretti et al., 2020a).

## 2.3 Magma storage at La Soufrière de Guadeloupe

Moretti et al. (2020a) proposed a model that describes the magma reservoir based on the crystal mush model, used at many similar systems to explain observations and activity (e.g., Cashman et al., 2017). This was refined by Metcalfe et al. (2021a), Metcalfe et al. (2021b); Metcalfe et al. (2022) to include a vertically and laterally extensive mush system extending 6–9 km in depth, which hosts relatively evolved magmas. A mush system is formed from repeated intrusions from depth and is composed of an interlocking framework of crystals with the presence of melt, containing dissolved volatiles, distributed in varying volumetric proportions within the network of crystals (e.g., Cashman et al., 2017). Remobilization of this mush system to produce eruptible magma may occur through the injection of mafic magma from depth into the shallow system, resulting in magma mixing. Alternatively, in eruptions where no mixing textures are observed (e.g., 1657 CE) exsolved fluids and heat from magma at depth may allow remobilization with no interaction with a mafic magma. Investigation of major and volatile elements of melt inclusions across several Holocene eruptions of La Soufrière shows the composition of the storage zone has remained stable during this time period (Metcalf et al., 2022). Melt inclusions (MI) from La Soufrière, and the neighbouring monogenetic cone of Echelle, range from 58–79 wt% SiO<sub>2</sub>, with major elements showing no systematic changes across the Holocene eruptions (Poussineau, 2005; Boudon et al., 2008; Pichavant et al., 2018; Metcalfe et al., 2022; Metcalfe et al., 2023).

Eruptions at the La Soufrière system have been shown through diffusion timescale studies to occur <1 year following remobilisation of the magma mush reservoir (e.g., by recharge of a more mafic magma) (Pichavant et al., 2018; Metcalfe et al., 2021a; 2021b). Understanding the trigger behind eruptive processes and the role volatiles play in these processes is particularly important given the short timescales. The rapid remobilisation of the mush system and potential short period of volcanic unrest, which may rapidly accelerate, makes crisis management and evacuation planning very important (Metcalf et al., 2021a; Metcalfe et al., 2021b). In order to make volcanic surveillance and crisis management most effective, we must understand clearly the processes leading to an eruption, including degassing dynamics and processes.

## 3 Methods

### 3.1 Sample collection and preparation

The samples used for this study were collected between 2001 and 2019, from both distal and proximal outcrops around La Soufrière.

The units were sampled across the entire thickness of the layer (channel sample) at constant depth to ensure the sample is representative of the whole unit. Samples from the 1657 CE, 1010 CE and 5680 BCE were taken from pumice fallout units, and the 341 CE sample was collected from a recent slump estimated to be from the upper and outer parts of the cone. This rain-triggered slump was found along the road at the base of the Echelle cone and allowed us to obtain the least altered deposits (Metcalf et al., 2021a; Metcalfe et al., 2021b; Metcalfe et al., 2022; Metcalfe et al., 2023). Detailed sample descriptions are available in Komorowski et al. (2005), Komorowski et al. (2008), Boudon et al. (2008), Legendre (2012) and Metcalfe et al. (2022), and for full stratigraphic context Legendre (2012) should be referred to. Stratigraphic context for the 1530 CE sample is from Komorowski et al. (2005), Poussineau (2005), Boudon et al. (2008), and Pichavant et al. (2018). All samples were treated and prepared using the same methods.

A selection of pyroxene and plagioclase crystals, which had been hand separated from the 500 µm sieved fraction, were also mounted in crystal bond. These crystals were partially polished in order to select crystals that hosted MIs. For Electron Micro-Probe analysis (EMPA), MIs were mounted in individual epoxy filled rings and polished individually using silicon carbide polishing pads sequentially in the following grades: P-800, P-1200, P-2400 and P-4000 and finished using 0.3 µm aluminium powder. The prepared inclusions were then carbon coated for EMPA. In order to avoid carbon contamination for CO<sub>2</sub> determination via Secondary Ion Mass Spectrometry (SIMS), a selection of MIs were prepared separately (Rose-Koga et al., 2021). Plagioclase and pyroxene crystals were mounted in crystal bond and polished using aluminium powder (3 µm, 1 µm and 0.3 µm), and crystals with melt inclusions were then pressed into indium and gold coated. Following SIMS analysis, this coating was removed and re-coated in carbon for major, F, S and Cl elements (EMPA, see section 3.2). Groundmass glass was selected, mounted in epoxy, polished and carbon coated using the same technique as for minerals and MIs for SEM.

### 3.2 Sample analysis

EMPA of major element (Si, Ti, Al, Fe, Mn, Mg, Ca, Na and K) and volatile (F, S and Cl) compositions of MIs, GM and minerals were obtained using the Cameca SX-100 and SX-5 which are part of the CAMPARIS platform at University Pierre and Marie Curie. Minerals were analysed using a 15 KV accelerating voltage, a beam current of 10 nA and a focused beam diameter of 1 µm. Glasses were analysed using a 15 KV accelerating voltage, a beam current of 10 nA (for Si, Ti, Al, Fe, Mn, Mg, Ca, Na and K) or 50 nA (S, Cl and F) and a defocused beam of 5 µm. In order to reduce the loss of Na, this element was analysed first, with the beam regularly blanked with a Faraday cup. The increased current and increased acquisition time used for S, Cl and F insured minimal loss for the volatile elements. However, the detection limit for F is relatively high at 150 ppm (Rose-Koga et al., 2021), such that the F concentration was below the detection limit for many inclusions. Moreover, F analysis is less precise because of the overlap of the FKα peak by the FeLα peaks (Lowenstern, 1994; Todd, 1996; Witter and Kuehner, 2004). EMPA standards and errors are reported in Table S1.

SIMS analysis was conducted using the Cameca IMS 1270 ion microprobe at the Centre de Recherches Pétrographiques et Géochimiques using a 10kV Cs<sup>+</sup> primary beam of 3 nA. This was used to measure H<sub>2</sub>O, CO<sub>2</sub>, S, Cl and F concentrations of the inclusions. Samples were pre-sputtered in order to reduce surface contamination reaching the mass spectrometer.

In addition to volatiles, we also measured deuterium (D) as a D/H isotope ratio, in order to assess the degree of H<sup>+</sup> diffusion which is used as a proxy for H<sub>2</sub>O loss in ~40 representative inclusions. The D/H ratio was calibrated using ETNA-0, TAN25-0, TAN25-2 and values are reported as δD, which is the per mil deviation of the D/H isotope ratio from the D/H ratio of Standard Mean Ocean Water (δD<sub>SMOW</sub>).

### 3.3 Data processing

The petrologic method was developed by Devine et al. (1984) and considers the volatile composition dissolved at depth and the remaining volatile content following degassing during an eruption. As this method does not involve direct measurements of emissions, this leads to some uncertainties when using this method, including: i) uncertainties in the volume of degassed magma, ii) underestimation of the volatile content in magma at depth determined by melt inclusions (MIs; Wallace, 2005; Moune et al., 2007; Venugopal et al., 2020), iii) the separation and co-existence of an immiscible sulphide phase and/or S-rich minerals, and iv) the partition into a pre-eruptive vapour phase if the magma is vapour saturated. Although direct measurements of emissions will always be more accurate (e.g., using remote sensing, Carn et al., 2016), the petrologic method is the only option to estimate emissions from past eruptions:

For each eruption we use the maximum MI volatile content (which represents pre-eruptive magma composition), the groundmass (GM) volatile content (which represents the post-eruptive magma composition; e.g., Moune et al., 2007; Zurek et al., 2019) and the estimated mass of the eruption (from Komorowski et al., 2008; Legendre, 2012; Esposti-Ongaro et al., 2020):

$$(X_{(max.MI)} - X_{(av.GM)}) \times volume \times density = X_{(emission)}$$

(Where X is a volatile species, e.g., S, Cl, F).

A minimum degassing must be assumed here because the petrologic method does include volatile contributions from unerupted magma at depth and the eruption masses are a minimum estimate calculated by Legendre (2012) using VEI.

We used the SOLWCAD and CHOSETTO v1 models to understand degassing processes in the magma of La Soufrière (Moretti et al., 2003; Moretti and Papale, 2004; Papale et al., 2006; Papale et al., 2022; see also Supplementary Table S2). SOLWCAD (available at <https://www.pi.ingv.it/progetti/eurovolc/>; last accessed on 5 December 2022) codes the Papale et al. (2006) models the saturation surface of a H<sub>2</sub>O and CO<sub>2</sub> in a melt of given composition. Hence for a given constant FeO/Fe<sub>2</sub>O<sub>3</sub> ratio along with a precise assessment of the onset of exsolution pressures (≈PH<sub>2</sub>O+PCO<sub>2</sub>), the total (gas + melt) amounts of these volatiles in the system can be calculated. For such reason, it can be used in a reverse mode to estimate saturation pressures back to the onset of exsolution from

sets of melt inclusion data (see Metcalfe et al., 2023 for application to Lesser Antilles Arc magmas). CHOSETTO, extends SOLWCAD to compute forward degassing of H<sub>2</sub>O, CO<sub>2</sub>, SO<sub>2</sub> and H<sub>2</sub>S in magmatic melts and also has the feature of consistently computing the relation between oxygen fugacity (*f*O<sub>2</sub>) FeO/Fe<sub>2</sub>O<sub>3</sub> redox ratio and how this affects the amounts of sulphur dissolved as sulphide and sulphate and so, the S-redox ratio. This allows us to expand the study of H<sub>2</sub>O-CO<sub>2</sub> degassing in order to understand the impact of S and the role of total volatiles on the degassing trends. Based on sulphur plus iron redox (Ottonello et al., 2001; Moretti and Ottonello, 2003; 2005; Moretti, 2005) H<sub>2</sub>O+ CO<sub>2</sub> models (Papale et al., 2006), the model has proved useful to interpret degassing at many volcanic sites spanning a quite large range of magma composition and geodynamic contexts (Aiuppa et al., 2007; 2010; 2017; Edmonds and Herd, 2007; Marini et al., 2011; Oppenheimer et al., 2011; Pino et al., 2011; Moretti et al., 2013a; Moretti et al., 2013b; de Moor et al., 2016; Moretti et al., 2018; Aiuppa et al., 2022). The program can be downloaded from <https://github.com/charlesll/chosetto> (DOI: 10.5281/zenodo.5554941).

To calculate the stratospheric aerosol optical depth (SAOD) perturbation and radiative forcing produced by the studied eruptions, we used EVA\_H (Easy Volcanic Aerosol\_Height), a simple model of volcanic sulphate aerosol forcing (Aubry et al., 2020). EVA\_H is an empirical box model predicting the temporal and spatial variation of aerosol optical properties given the characteristics of a volcanic SO<sub>2</sub> injection (mass, latitude, altitude, and season). It was calibrated for the 1979–2015 eruption sequence using recent satellite based volcanic SO<sub>2</sub> emission inventories (Carn et al., 2016) and stratospheric aerosol optical properties observations (Thomason et al., 2021). The SAOD at 550 nm predicted by EVA\_H is converted into an effective radiative forcing at the top of the atmosphere using the tropical eruption scaling from Marshall et al. (2019).

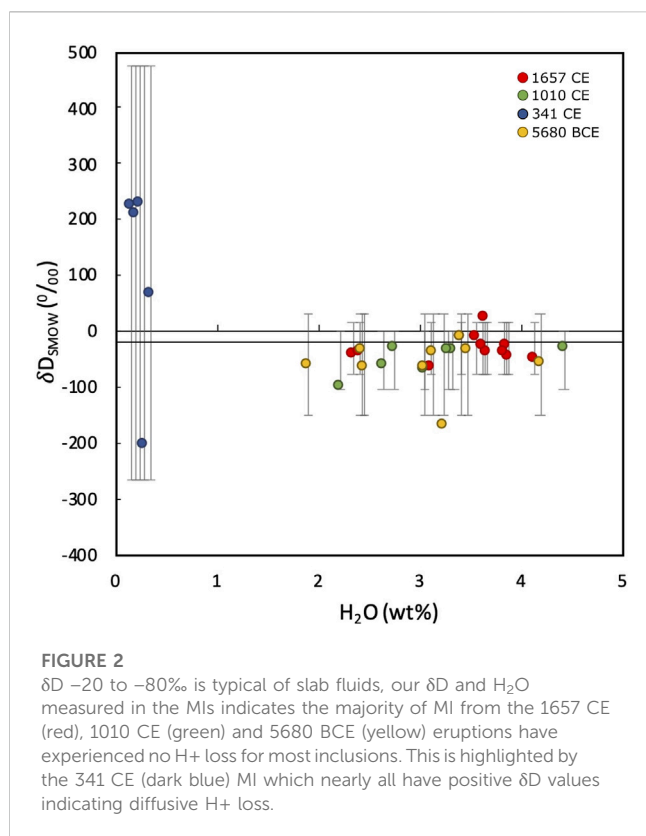
## 4 Results

### 4.1 Volatiles

For a full report of major element analysis for MI and GM please refer to Metcalfe et al. (2022) and Metcalfe et al. (2022). A summary of key geochemical data is provided in Table 1. MIs in this dataset have not experienced any post-entrapment crystallization, and are in equilibrium with their host mineral (Putirka, 2008). Additionally, no bubbles were observed in the MIs.

To understand whether the volatile elements in the MI are representative of the undegassed magma, particularly if any H<sub>2</sub>O loss has occurred from the inclusions, we measured the D/H ratio of the MI. The D/H ratio is expressed as δD (the permil deviation from Standard Mean Ocean Water (δD<sub>SMOW</sub>)). Slab fluids related to the average upper MORB mantle fall in the range δD −20 and −80‰ and values below −150‰ are the upper limit of terrestrial mantle values (Shaw et al., 2008).

The 1657 CE, 1010 CE and 5680 BCE MI all fall within this δD −80 to −20‰ range, which indicates the trapping of variably degassed melts has occurred rather than post-entrapment H<sub>2</sub>O loss (Figure 2). However, the majority of the 341 CE eruption inclusions have a large range of positive values (δD 50‰–290‰; Figure 2).



Positive  $\delta D$  values indicate loss of hydrogen, either by secondary degassing of H-bearing molecules or diffusive loss, addition of seawater and/or secondary hydrothermal alteration (Kyser and O'Neil, 1984; Hauri, 2002; Portnyagin et al., 2008; Shaw et al., 2008; Métrich and Deloule, 2014). This shows the 341 CE inclusions have experienced  $H_2O$  loss, which explains the very low  $H_2O$  values recorded. This shows that we can use the 1657 CE, 1010 CE and 5680 BCE  $H_2O$  data as these can be interpreted as variably degassed melts, but the 341 CE data cannot be used as they have experienced post-entrapment  $H_2O$  loss and do not represent the  $H_2O$  content of the melt originally trapped.

Here, we report the MI volatile dataset plotted against the incompatible element  $K_2O$  and also report the average GM value for each eruption to understand the effects of crystallization and degassing (Figure 3A). The  $H_2O$  values measured for this study range from 1.05–4.42 wt% (excluding values from 341 CE). The  $H_2O$  values for 1530 CE calculated by difference extend this range to 5.6 wt% (Pichavant et al., 2018) however, based on the SIMS data from the other eruptions discussed here this is perhaps an overestimate.

$CO_2$  for this study ranges from 2070 ppm to below the detection limit, with the highest  $CO_2$  values recorded in the 341 CE eruption (Figure 3B). The upper values above 1700 ppm may be outliers with most of the 341 CE  $CO_2$  data falling below 1,500 ppm, the  $H_2O$  loss observed from these inclusions also makes it unclear if  $CO_2$  has also been affected. A clear trend of decreasing  $CO_2$  with increasing  $K_2O$  is observed, which could relate to ascent and crystallisation of the magma, assuming incompatible behaviour (Blundy and Cashman,

2008). Alternatively, this could also relate to the effects of decompression on magmas in a polybaric storage zone (Blundy and Cashman, 2008). No distinction is made between  $CO_2$  and the eruption style (Metcalf et al., 2022); however, the 341 CE Strombolian eruptions records distinctly higher  $CO_2$  contents.

The Cl data range from 0.10–0.36 wt% and the data are relatively clustered in comparison to the other volatiles with no clear correlation with  $K_2O$  (Figure 3C). The GM values again generally show lower  $K_2O$  and lower Cl than the MI (0.16–0.18 wt%); however, for the 341 CE eruption the GM Cl is notably lower (0.02 wt%), with no overlap between MI and GM data (Figure 3C). S data range from <780 ppm to below the detection limit and show a weak positive correlation, with S increasing with increasing  $K_2O$  (Figure 3D). The average GM values range from 100–225 ppm and fit into this trend, with lower  $K_2O$  and lower S values than many of the MI. F data range from 680 ppm to below the detection limit, with values below 100 ppm considered to be below the detection limit (Figure 3E). The data above the detection limit show a weak positive correlation. Generally, the F values for the GM is ca. 100 ppm; however, for the 341 CE eruption the GM shows similar F values to the MI (410 ppm). The 1530 CE GM F content is also higher than the other La Soufrière eruptions (200 ppm). No clear relationship is observed between eruption style and halogen content.

## 4.2 Volatile emissions

In order to estimate the volatile flux from past eruptions, we used the petrologic method (Devine et al., 1984) which compares the dissolved volatile content in MI to the GM volatile content (Table 1), scaled to the eruption volume with a rock density of  $2,450 \text{ kg/m}^3$  for all eruptions (calculated using a linear inversion of gravimetric data by Barnoud et al., 2016). As density values are not available for the individual eruptions, we chose to use the same density value for all eruptions. However, as the 341 CE eruption is more basaltic in composition than the 1657 CE, 1530 CE, 1010 CE and 5680 BCE eruptions this may increase the error on calculations for this eruption. Estimated eruption volumes are calculated by Legendre (2012) and are the main source of error in the calculation of volatile emissions (Table 1). Volumes calculated by Legendre (2012) use VEI (Newhall and Self, 1982) which integrates total volume of tephra erupted, height of eruptive column and duration of event with eruptive type, eruptive style to provide the relative size and magnitude of the eruptions. Given the lack of outcrops and erosion which has occurred this provides the best estimate of volume; however, this leaves large uncertainties which are difficult to assess. Legendre (2012) chose to report the minimum erupted volume value, this means any estimates of volatile emissions should also be considered a minimum. As discussed earlier; the 1530 CE sub-plinian eruption is the only one for which volumes have a known range (ca. 0.07 to  $0.09 \text{ km}^3$ ).

Overall, the larger Plinian (VEI 4) eruptions have higher emissions as expected (Table 2). The 1010 CE eruption has the highest total volatile emissions (11.6 Mt) which is comparable to the 5680 BCE eruption (11.3 Mt), the 1657 CE and 341 CE eruptions have considerably lower total emissions at 0.11 and 0.02 Mt, respectively (Table 2). We also calculated total emissions for the 1530 CE using the  $H_2O$  value calculated by difference from

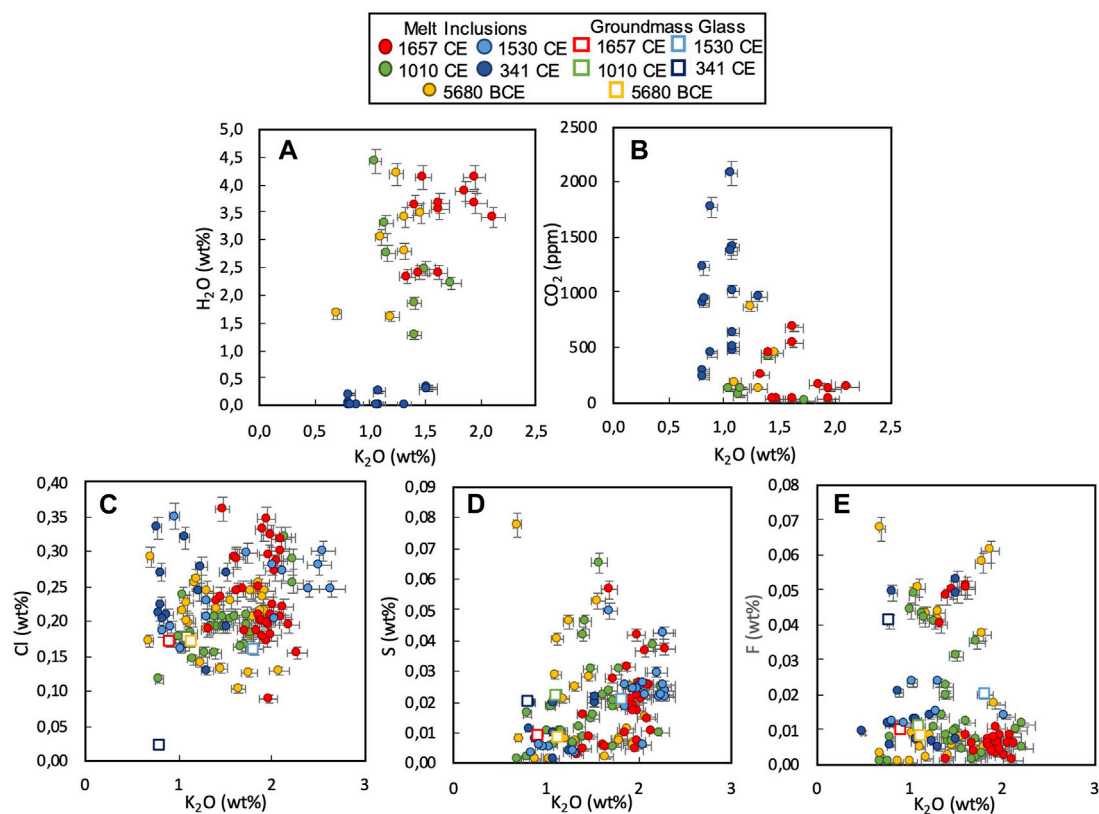


FIGURE 3

(A) H<sub>2</sub>O; (B) CO<sub>2</sub>; (C) Cl; (D) S; (E) F vs. K<sub>2</sub>O for melt inclusion (MI—circles) and average groundmass (GM—open squares) for the eruption series. The 341 CE inclusions have lost H<sub>2</sub>O so the data does not follow the trends of the La Soufrière MI. In comparison, the 341 CE CO<sub>2</sub>, S and Cl data appears to fit with the trend from the other eruptions, F data however, is generally below the detection limit. 1530 CE data is supplemented with data from [Poussineau, 2005](#); [Boudon et al., 2008](#); [Pichavant et al., 2018](#).

[Pichavant et al. \(2018\)](#). This gives total emissions of 12.8 Mt, which is higher than both Plinian eruptions studied and can be considered an outlier, which could be explained by the method used to obtain the water concentration. Indeed, the by difference method (e.g., [Kilgour et al., 2016](#)) is known to be less accurate and precise than actual H<sub>2</sub>O concentration measurements.

As SO<sub>2</sub> is one of the most important volatiles emitted due to its impact on the climate, SO<sub>2</sub> emissions have also been calculated. The emissions of SO<sub>2</sub> also constitute a relatively minor component in the 1657 CE, 1530 CE and 341 CE eruptions and ranges from 0.0001–0.002 Mt of SO<sub>2</sub> ([Table 2](#)). When using a higher density (2,685 kg/m<sup>3</sup>; [Komorowski et al., 2008](#)) to calculate emissions for the more basaltic eruption we observe a negligible increase in SO<sub>2</sub> emissions (increase of 6.7x10<sup>-6</sup> Mt). SO<sub>2</sub> emissions are higher in the two Plinian eruptions, with the 1010 CE eruption emitting 0.2 of Mt SO<sub>2</sub> and the 5680 BCE eruption emitting 0.3 Mt of SO<sub>2</sub>. HCl emissions are higher with the two Plinian (VEI 4) eruptions which both emitted 0.3–0.4 Mt of HCl. 1530 CE also has a high HCl emission at 0.4 Mt of HCl, in comparison to 1657 CE and 341 CE eruptions which emitted 0.005 and 0.008 Mt respectively of HCl. Finally, HF emissions are only a relatively minor component ranging from 0.0003–0.08 Mt of HF, except in the 5680 BCE eruptions which has a HF emission of 0.2 Mt of HF ([Table 2](#)).

## 5 Discussion

### 5.1 Degassing processes at La Soufrière de Guadeloupe

#### 5.1.1 SOLWCAD and CHOSETTO modelling

First, we investigated the H<sub>2</sub>O–CO<sub>2</sub> degassing for the 1657 CE, 1010 CE and 5680 BCE eruptions, for which we have SIMS H<sub>2</sub>O and CO<sub>2</sub> measurements with no clear volatile loss observed. To investigate H<sub>2</sub>O–CO<sub>2</sub> degassing and the onset of exsolution the SOLWCAD program is used, which calculates saturation isobars and then open and closed degassing paths at various H<sub>2</sub>O<sub>(total)</sub> and CO<sub>2</sub> <sub>(total)</sub> during degassing ([Figure 4](#)) for a constant melt composition, i.e., for a given FeO/Fe<sub>2</sub>O<sub>3</sub> ratio. We started our model at the highest H<sub>2</sub>O and CO<sub>2</sub> contents analysed (a 5680 BCE MI with 4.2 wt% H<sub>2</sub>O and 900 ppm CO<sub>2</sub>). The degassing paths highlight the spread in the MI data both across all the eruptions studied and within the individual eruptions. Though some data points, particularly from the 1657 CE eruption lie close to the closed system degassing path scenarios, it is unlikely that a simple closed or open degassing path can be used to explain the variability in the MI data. Instead, these data is better explained by the eruption being supplied from variably degassed

TABLE 2 Results of the petrologic method.

| Volatiles            | Total*  |      |      |       |      | SO <sub>2</sub> |       |       |         |       | HCl     |       |       |         |       | HF      |        |       |         |       |   |
|----------------------|---------|------|------|-------|------|-----------------|-------|-------|---------|-------|---------|-------|-------|---------|-------|---------|--------|-------|---------|-------|---|
|                      | 1657    | 1530 | 1010 | 341   | 5680 | 1657            | 1530  | 1010  | 341     | 5680  | 1657    | 1530  | 1010  | 341     | 5680  | 1657    | 1530   | 1010  | 341     | 5680  |   |
| Eruption             | -       | -    | -    | -     | -    | -               | -     | -     | -       | -     | -       | -     | -     | -       | -     | -       | -      | -     | -       | -     | - |
| % of degassing       | -       | -    | -    | -     | -    | 85              | 58    | 66    | 7       | 89    | 52      | 53    | 48    | 93      | 41    | 81      | 14     | 73    | 24      | 88    |   |
| Emissions (Mt)       | 0.1     | 12.8 | 11.6 | 0.02  | 11.3 | 0.002           | 0.001 | 0.2   | 0.0001  | 0.3   | 0.005   | 0.4   | 0.4   | 0.008   | 0.3   | 0.001   | 0.0001 | 0.08  | 0.0003  | 0.2   |   |
| Emissions Error (Mt) | ±0.0007 | ±3   | ±0.7 | ±0.09 | +0.2 | ±0.0001         | ±0.01 | ±0.02 | ±0.0001 | ±0.02 | ±0.0005 | ±0.04 | ±0.04 | ±0.0004 | ±0.04 | ±0.0001 | ±0.003 | ±0.05 | ±0.0001 | ±0.01 |   |

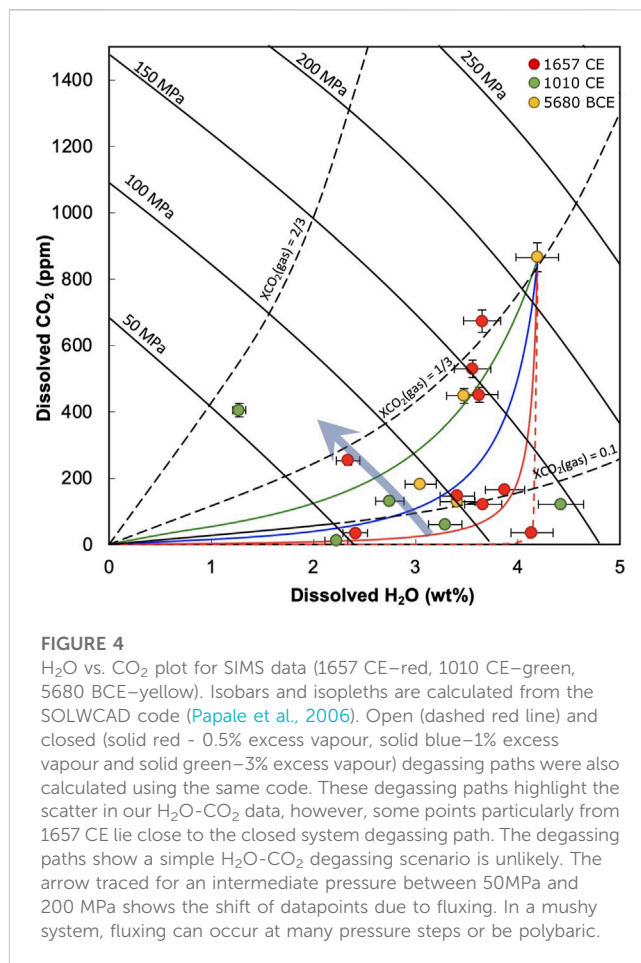


FIGURE 4 H<sub>2</sub>O vs. CO<sub>2</sub> plot for SIMS data (1657 CE—red, 1010 CE—green, 5680 BCE—yellow). Isobars and isopleths are calculated from the SOLWCAD code (Papale et al., 2006). Open (dashed red line) and closed (solid red - 0.5% excess vapour, solid blue—1% excess vapour and solid green—3% excess vapour) degassing paths were also calculated using the same code. These degassing paths highlight the scatter in our H<sub>2</sub>O–CO<sub>2</sub> data, however, some points particularly from 1657 CE lie close to the closed system degassing path. The degassing paths show a simple H<sub>2</sub>O–CO<sub>2</sub> degassing scenario is unlikely. The arrow traced for an intermediate pressure between 50 MPa and 200 MPa shows the shift of datapoints due to fluxing. In a mushy system, fluxing can occur at many pressure steps or be polybaric.

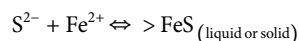
melts within a mush system. In particular, degassing paths may reflect the CO<sub>2</sub>-enrichment due to the fluxing of shallower magma layers by the deep gas released from deeper levels in the magmatic system (Figure 4). This effect is commonly observed in almost all sets of melt inclusions from worldwide volcanoes (e.g., Métrich and Wallace, 2008; Blundy et al., 2010; Caricchi et al., 2018; Moretti et al., 2018), including those of the Lesser Antilles Arc (Metcalfe et al., 2023).

To further understand degassing processes in the presence of sulphur, we then use CHOSETTO v1, which is an extended version of SOLWCAD in forward mode (Moretti and Ottonello, 2003; Moretti and Papale, 2004). The average MI composition used comes from the 5680 BCE eruption (which has the highest MI S content) and is saturated with the highest total volatiles recorded across the geochemistry series (CO<sub>2</sub> is the highest repeated value from 341 CE). We ran the same compositions and conditions at multiple oxidation states (NNO+0.8, NNO and NNO-0.5) under open and closed system conditions. This is important when investigating S as the partitioning of sulphur depends on redox conditions, with the sulphur partition coefficient increasing with increasing *f*O<sub>2</sub> (e.g., Scaillet et al., 2012). Although the degassing paths under open conditions at NNO-0.5 conditions (Figure 5) fit closer to the dataset, this does not produce the steep decrease in sulphur over a small range of S contents (Figure 5) as long as the highest S-content is taken as the initial (total) value (Figure 5A).

We then interpret the vertical drop in S over a constant H<sub>2</sub>O across the different magmas as evidence for early S-separation. Such a drop was also necessary to effectively model degassing at Mt. Mazama (Marini et al., 2011) and Mt. Etna (Moretti et al., 2018). At sulphide saturation, a S-bearing phase will separate from the melt (e.g., as minerals such as pyrrhotite, chalcopyrite, anhydrite; as an immiscible liquid and/or as a vapour phase). Given the range of oxidation states adopted here and the evidence that FeS separation occurs in many magmatic suites falling in this range (Luhr et al., 1984; Williams et al., 1990; Andres et al., 1991; Gerlach and McGee, 1994; Wallace and Gerlach, 1994; Gerlach et al., 1996; Scaillet et al., 1998; Collins et al., 2012; Mungall et al., 2015; Yao and Mungall, 2020), we opt for early S-loss due to FeS separation. No S-rich minerals or sulphide globules are observed in the eruption products, as they may have segregated at depth into cumulate layers due to density differences or be resorbed during sulphur degassing. Moreover, no bubbles are observed in the MIs, suggesting that the hypothesis of the presence of a S-rich vapour phase could be ruled out.

### 5.1.2 Fe-S separation

S is removed from the magma by loss of S<sup>2-</sup> via sulphide separation as liquid FeS at magmatic temperatures (Marini et al., 2011; Moretti, 2021):



Sulphide precipitation results in patchy sulphur distribution through the magma and requires the calculation of the sulphur budget (S dissolved in the magma, S dissolved in the sulphide phase and exsolved S) over a large volume of the magma which cannot be approximated by the limited volume involved in MI. Phase separation is considered an important mechanism (Lester et al., 2013), that allows many natural magmas to co-exist with an immiscible liquid sulphide phase or pyrrhotite (Moretti and Baker, 2008; Jenner, 2017; Yao and Mungall, 2020).

Sulphide saturation and separation is an important process in arc magmas, which occurs within the mush zones prior to magma ascent (Jenner, 2017). Due to the immiscibility of the FeOS liquid and the silicate magma this can result in the concentration of FeS-droplets, the resulting liquids separate due to density differences (Collins et al., 2012). The Fe-S droplets are denser than the silicate magmas and so settle with cumulate phases at the base of the system, which prevents them from being readily sampled, including by melt inclusions, as shown by the La Soufrière samples. Alternatively, the interaction between Fe-S droplets and vapour bubbles may allow their flotation. This could provide a mechanism to transport sulphides through to shallower levels of the magma system and account for the release of excess S if sulfide resorption occurs to release S back into the melt+vapour system (Mungall et al., 2015; Edmonds and Mather, 2017; Lee and Tang, 2020; Yao and Mungall, 2020). This increases the complexity of understanding the S budget at this system, particularly when considering the S emissions at the surface.

Our data show a systematic decrease in S over time which indicates the whole system is evolving by separating FeS, which results in a decrease in S content from the oldest magma suite to the youngest. Understanding the values of sulphide saturation depends

on where in the system, and at which point of magma differentiation, sulphide separation occurs. S solubility and saturation vary between melt composition, particularly the FeO content of the melt and pressure (Carroll and Rutherford, 1985; Moretti and Baker, 2008). We therefore estimate the sulphur concentration for the 1657 CE, 1010 CE and 5680 BCE magmas using the equation presented by Liu et al. (2007) to estimate the sulphur concentration of silicate melts at sulphide saturation (SCSS) as the MIs are not water saturated (e.g., Moune et al., 2007). Liu et al. (2007) constructed a model to predict SCSS in magmas ranging from basalts to rhyolites with a range of water contents. This model predicts SCSS in the 1657 CE, 1010 CE and 5680 BCE magmas occurs between 0.15–0.3 wt% S. This is higher than measured in the melt inclusions and indicates a larger S drop has occurred than observed in the data.

At La Soufrière we will consider the system must experience continuous FeS separation to produce the evolved magma batches, which are characterized by different initial S contents. We therefore initiate our degassing model after sulphur separation in the deeper system, to understand the shallow system degassing behaviour. This allows us to demonstrate degassing models from both high S (900 ppm) and low S (<500 ppm) with the difference between these two values produced by FeS separation (e.g., Marini et al., 2011).

Our shallow degassing models investigate the average 1657 CE, 1010 CE and 5680 BCE MI composition; however there is only a small variation in the average MI compositions, so this has a minimal effect on the degassing paths produced. The volatiles used for each scenario are shown in Supplementary Table S2. We used the maximum H<sub>2</sub>O and CO<sub>2</sub> measured in each eruption, except for the 1010 CE eruption which we used 900 ppm (as in the 5680 BCE scenario), as CO<sub>2</sub> was too low to allow saturation.

### 5.1.3 fO<sub>2</sub> behaviour

Each scenario was decompressed from the pressure calculated from the MIs, as shown in Supplementary Table S2. We ran the same compositions and conditions at multiple oxidation states (NNO+0.8, NNO and NNO-0.5) under open and closed system conditions (where NNO is the nickel-nickel-oxide buffer). The upper limit oxidation state is taken from experimental results conducted by Pichavant et al. (2018), while the lower limit is required by the data. Decompression under these conditions allows us to demonstrate the shallow degassing path of S. Degassing occurring from a starting point of 450 ppm S under NNO to NNO-0.5 fits the trend of our data well (Figure 5). However, under more oxidised conditions (NNO+0.8) the degassing path does not fit the trend observed in the data, with the model showing S remaining relatively high decreasing with H<sub>2</sub>O in comparison to the data (Figure 5). This is also observed starting from 350 ppm S, with degassing paths at NNO-0.5 fitting the data (Figure 5). At lower S contents (250 ppm), more oxidised degassing paths appear more feasible (Figure 5).

Alternatively, we could adopt a unique relative oxygen fugacity (i.e., constant ΔNNO value) and consider that CO<sub>2</sub>-enrichment due to fluxing (Figure 4) would shift the degassing trend to low H<sub>2</sub>O-contents, as proposed by Moretti et al. (2018) for Mt. Etna. Nevertheless, our data do not allow a clear distinction between the effects due to fluxing and those due to varying oxygen fugacity. We

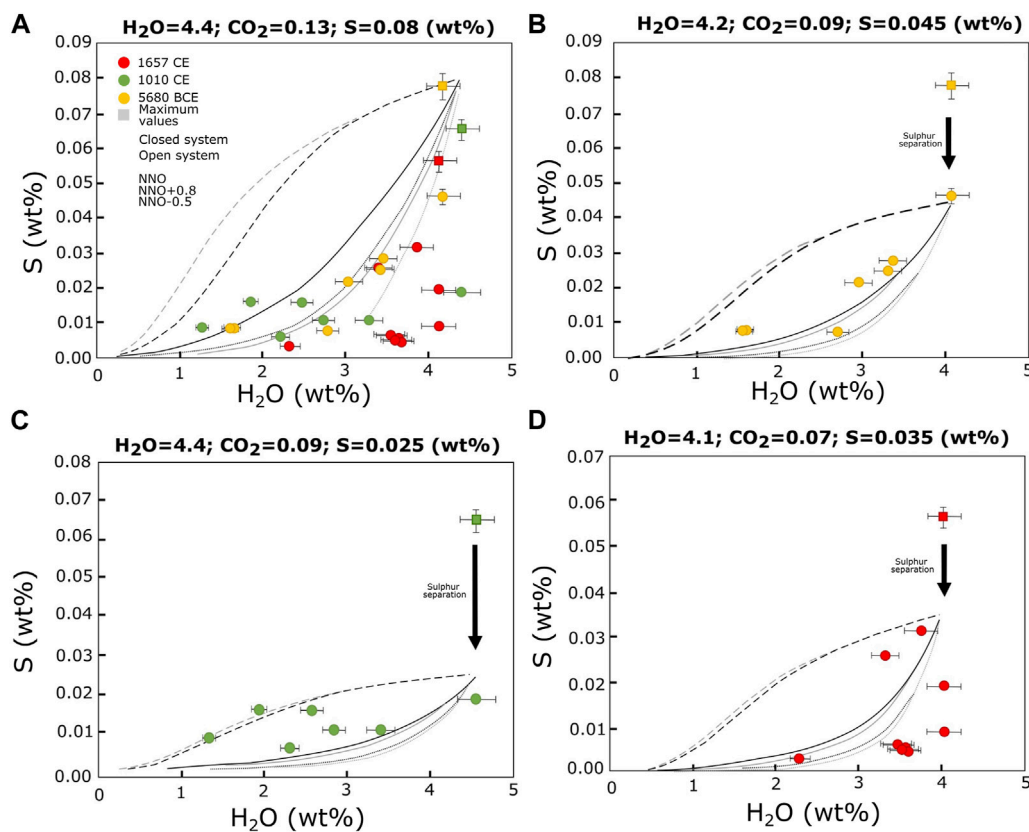


FIGURE 5

S vs.  $H_2O$  graphs showing open system (grey) and closed system (black) degassing paths calculated by CHOSETTO at NNO+0.8, NNO and NNO-0.5.

(A) Decompression of 5680 BCE MI composition, this is unable to reproduce the vertical drop in S using simple degassing paths. Following initial sulphide separation: (B) Decompression of 5680 BCE composition; (C) Decompression of a 1010 CE composition; (D) Decompression of 1657 CE composition. (Square symbol = Maximum values recorded by MI, arrows showing the change in composition due to sulphide separation).

speculate that the heterogeneity of magma distribution within a mushy plumbing system creates a variety of magma parcels each ruled by its own initial volatile content and oxygen fugacity.

Overall, the model reproduces reasonable degassing paths related to decompression at low pressures, suggesting the majority of S degassing has occurred during magma ascent. The results of this model indicate more reduced conditions than proposed by Pichavant et al. (2018), which is expected if FeS precipitation occurs. However, this may relate to variations within the mush system, with the more oxidised conditions modelled by Pichavant et al. (2018) relating to the deeper system (e.g., Pichavant et al., 2018), whereas the more reduced conditions modelled here would relate to shallower portions of the system. The changes related to decompression degassing and sulphide separation would result in a decrease in  $fO_2$  to more reduced conditions, as modelled here and also reported by a wide literature. Progressive changes of oxygen fugacity during degassing have in fact been modelled and observed for several systems (e.g., Anderson and Wright, 1972; Candela, 1986; Carmichael and Ghiorso, 1986; Burgisser and Scaillet, 2007; Métrich et al., 2009; Gaillard et al., 2011; 2015; Oppenheimer et al., 2011; Kelley and Cottrell, 2012; Moussallam et al., 2014; Moussallam et al., 2016; Brounce et al., 2017). There is then consensus the  $fO_2$  of the magma after degassing will not represent the  $fO_2$  of the initial melt, unless recent forward

models (Hughes et al., 2022) show that degassing begins near the sulphur-solubility minimum, which is defined with respect to  $fO_2$  and represents an important boundary of some models (Moretti et al., 2003; Cicconi et al., 2020; Hughes et al., 2022).

A decrease in  $fO_2$  from oxidised conditions to reduced conditions has also been reported at Etna (Gennaro et al., 2020) and Kilauea (Moussallam et al., 2017). The exact mechanism promoting this change appears to be specific to each magmatic setting. At Kilauea, this decrease was related to sulphur degassing without the involvement of  $H_2O$  and  $CO_2$  (Moussallam et al., 2017). At Etna, the  $fO_2$  decrease was instead related to compositional evolution, primarily dehydration, and decreasing pressure (Moretti, 2022). A similar effect is modelled by Moretti and Ottonello (2022) for the experimental ferri-basalts synthesized and investigated by Botcharnikov et al. (2005), where water represents the main compositional variable.

However, the interpretation of different  $fO_2$  behaviours depends largely on adopted models, particularly the oxybarometers that are used to obtain and extrapolate  $fO_2$  as a function of pressure, temperature and melt composition (i.e., melt-driven interactions related to its structure or polymerization state) from measured redox pairs of iron and/or sulfur (Moretti and Stefansson, 2020; Moretti, 2021; Moretti, 2022). Despite magmatic differentiation and dehydration increasing the nominal abundance of oxygen in

magmas approaching the surface, the decrease of oxygen fugacity reflects the increase of melt polymerization and then the decrease of so called “free-oxygen” (i.e.,  $O^2$ ) (Moretti, 2022), whose activity is proportional to oxygen fugacity (Moretti, 2005; Cicconi et al., 2020a; Moretti, 2021; Moretti and Ottonello, 2022).

#### 5.1.4 Comparison to present day degassing

Allard et al. (2014) suggest the magma feeding the system of La Soufrière is open to basaltic replenishment at the base and to gas escape from the top, which supplies the hydrothermal emissions observed at the surface. The range of  $C/S_{(total)}$  measured by the Observatoire Volcanologique et Sismologique de Guadeloupe with different methods (soda bottles,  $P_2O_5$  bottles, MultiGas) across several years (2012–2022; Tamburello et al., 2019; Moretti et al., 2020a; Moretti et al., 2020b; Moune et al., 2022) ranges from 1 to 6, with a mean of 4 (Figure 5B in Moretti et al., 2020b). The vertically extensive plumbing system of La Soufrière involves the polybaric, multistep or even continuous degassing of magma from the main deep reservoir (ca. 5–9 km) up to the shallow reservoir (ca. 3 km) (Villemant et al., 2014; Moretti et al., 2020a). Therefore, the gas feeding the hydrothermal system at the top of the magma system results from multiple contributions that integrated over a large depth range.

We report the  $C/S_{(total)}$  values from our CHOSETTO v1 degassing simulations vs. depth in Figure 6. This shows large  $C/S_{(total)}$  ratios for the deep reservoir (8 km, 200 MPa), where the fresh magma has  $C/S_{(total)}$  varying from approximately 10 (NNO-0.5) to approximately 100 (NNO+0.8) (Table 1; Supplementary Table S2). For depths corresponding to the shallow reservoir (~3 km, ~75 MPa),  $C/S_{(total)}$  varies from approximately 1.5 (NNO+0.8, with open system degassing) to approximately 10 (NNO+0.08, with closed system degassing). The bracketed shaded area corresponds to the region at 3–6 km depth in which hydrothermal  $C/S_{(total)}$  (measured values range from 1 to 6; with a mean of 4; Moretti et al., 2020b) is released, feeding the overlying hydrothermal system. Six km is hypothesised to be the top of the main reservoir and above this is a crystal mush, though it is unclear if this area of the system is crystallised or in a mushy state. Considering that the gas released should integrate contributions from various depths across this vertically extended magma system, we also consider that the  $C/S_{(total)}$  hydrothermal values may be consistent with both degassing and the mixing between the deep system (200 MPa, 8 km) and shallow system (~75 MPa, 3 km) residual magmatic gases.

For the same oxygen fugacity mixing lines and closed system degassing patterns nearly overlap. However, as discussed above, it is highly plausible that a decrease in oxygen fugacity is observed with decreasing depth. Therefore, we plot on Figure 6 mixing lines connecting the gas composition from the deep oxidized (NNO+0.8) reservoir to a shallow but reduced magma (NNO-0.5). From Figure 6 we see that  $C/S_{tot}$  values presently measured at La Soufrière fumaroles are not compatible with degassing under oxidized reservoir (NNO+0.8), which produces gases with  $C/S_{tot}$  ratios that are significantly higher than those expected to occur within the shallow reservoir (grey rectangle in Figure 6). This suggests the magma degassing at about 3 km depth must be necessarily reduced ( $\log fO_2 < NNO$ ). The present-day gas is entering the hydrothermal system and then separating from a

magma emplaced and degassing under closed-system degassing between 3 and 6 km depth (shown by the 1657 CE and 5680 BCE models, the 1010 CE eruption, however has values consistent between 3 km and 5 km depth). Further mixing with the gas released by the deep oxidized magma at NNO+0.8 may contribute to the final composition in variable proportions.

These results should be taken cautiously, as they do not include the role of hydrothermal scrubbing, which will increase the  $C/S_{(total)}$ . These results also consider magmatic degassing driven uniquely by decompression, without accounting for crystallization, which in a mushy system leads to strong open system volatile differentiation in absence of decompression (e.g., Moretti et al., 2013a; Moretti et al., 2013b). Despite our approximations and limits discussed, the fumarolic  $C/S$  match reasonably well with those calculated from CHOSETTO for the magmatic gas input into the hydrothermal system (Figure 6). This suggests that the continuous flow-through of deep gas attains a steady state condition, such that the output fumarolic  $C/S$  ratio can be well approximated by the input magmatic  $C/S$  ratio. Under such a regime, the hydrothermal buffering of sulphur involving pyrite-like minerals (Giggenbach, 1988) does not alter significantly the bulk sulphur budget, as already shown for other hydrothermal-magmatic systems in a state of unrest such as Solfatara di Campi Flegrei, Italy (Moretti et al., 2013a; Moretti et al., 2017). In terms of monitoring, fluctuations of the fumarolic  $C/S$  ratio in the observed one to six range can instead be used as an indicator of hot and oxidized ( $CO_2$ - and  $SO_2$ -rich) gas pulses into the hydrothermal system (Moretti et al., 2020a).

## 5.2 Volatile emissions and climate forcing at La Soufrière de Guadeloupe

### 5.2.1 Volatile emissions at La Soufrière de Guadeloupe

More intense VEI 4 eruptions have higher total volatile emissions (Figure 7A). Eruptions with the same VEI have comparable total volatile emissions; this is due to the petrological method which requires scaling of the volatile concentration to erupted volume. A notable outlier is the 1530 CE eruption, which is due to the higher  $H_2O$  content reported by Pichavant et al. (2018) and estimated by difference. The diffusion timescales calculated by Metcalfe et al. (2021a), Metcalfe et al. (2021b), shows no correlation with the total volatile emissions of each eruption. The 1657 CE and 5680 BCE eruptions have comparable expected diffusion timescales (Metcalfe et al., 2021a; Metcalfe et al., 2021b); however, the total volatile emissions are very different (Figure 7B). The groundmass glass plus microlites viscosity, calculated by Metcalfe et al., 2022, correlates with the total volatile emissions, with a higher groundmass glass viscosity correlating with lower total volatile emissions (Figure 7C). This suggests lower viscosity in the groundmass glass allows for more degassing and higher volatile emissions. Faster ascent rates (calculated by Metcalfe et al., 2022 to range from <1–12 m/s at La Soufrière) correlate with higher total volatile emissions (Figure 7D). However, this is not observed in all the eruptions due to top-down effects, such as a reduction of permeability at the surface due to hydrothermal activity (e.g., Cassidy et al., 2018),

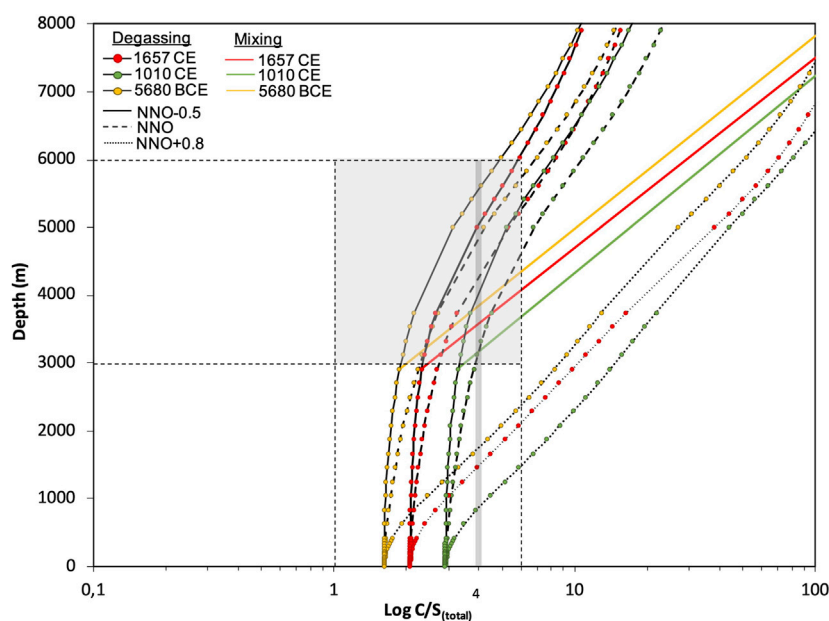


**FIGURE 6**

Model-based  $C/S_{(total)}$  ratios resulting from closed-system magmatic degassing under different oxygen fugacities for the three eruptions considered in this study. Also reported are the mixing lines of shallow and reduced with deep and oxidized gases. The bracketed shaded area corresponds to the region at 3–6 km depth in which current hydrothermal  $C/S_{(total)}$  (values are measured by multigas range from 1 to 6; with a mean of 4; Moretti et al., 2020a; Moretti et al., 2020b) is released, feeding the overlying hydrothermal system. With 6 km being the top of the main reservoir and above this is a crystal mush which is unclear has been crystallised, the  $C/S_{(total)}$  hydrothermal values may be consistent with the mixing between the deep system (200 MPa, 8 km) and shallow system (~75 MPa, 3 km) residual magmatic gases.

which have allowed slow ascending magmas to result in large eruptions.

In order to contextualise our results, we integrate the La Soufrière emissions into a global database of subduction zone volcanoes (Figure 8).  $SO_2$  data are readily available, this is also one of the most important volatiles emitted due to its impact on the climate (Graf et al., 1997; Robock, 2000; Textor et al., 2003; Oppenheimer et al., ; Timmreck, 2012; Macdonald and Wordsworth, 2017; Marshall et al., 2022). Hence, we focus on  $SO_2$  emissions, comparing our data to other systems where the petrologic method has been used to calculate  $SO_2$  emissions (Figure 8). It is important to consider that  $SO_2$  calculated using the petrologic method is usually lower than remote sensing measurements as described in Section 3.3 (e.g., Wallace, 2003). The collated data generally cover eruptions larger (>VEI 4) than those studied here; however, some data also exist for eruptions of lesser intensity. Although the petrologic method underestimates the quantification of volcanic emissions, Scaillet et al. (2003) provide a global database of  $SO_2$  emissions calculated using the petrologic method but also include a thermodynamic estimation to estimate the co-existing S-rich vapor phase at depth for intermediate to silica magmas (improved petrologic method; Figure 8). Scaillet et al. (2003) demonstrate the  $SO_2$  emissions calculated closely agree with independent estimates obtained from analysis of ice cores, optical-depth measurements, and remote-sensing spectroscopic techniques.

The VEI 4 5680 BCE and 1010 CE eruption  $SO_2$  emissions (0.3 and 0.2 Mt of  $SO_2$ , respectively) are very comparable to eruptions with similar magma volumes (e.g., Mount Unzen 1991 which emitted 0.25 Mt of  $SO_2$ ). Data available from the

Lesser Antilles eruptions Montagne Pelée 1902 (0.3 Mt of  $SO_2$ ) and Soufrière St Vincent 1979 (0.5 Mt of  $SO_2$ ) also have comparable  $SO_2$  emissions to those of the 5680 BCE and 1010 CE eruptions (Figure 8). The eruption of 1995 Soufrière Hills volcano, Montserrat, is less comparable due to a higher magma volume, but does give an indication of what  $SO_2$  emissions could be expected from a larger eruption from La Soufrière. It is notable that volatile emissions for the voluminous eruption of the Roseau Tuff on Dominica are much larger than those of any La Soufrière eruptions, despite being neighboring systems. The agreement of these different eruption  $SO_2$  estimates (Figure 8) indicates that our petrologic method using our maximum S values, which correspond to the sulfur in the magmas plus the separated sulfur phase (equivalent to the improved petrologic method from Scaillet et al., 2003), provides reasonable minimum estimates of  $SO_2$  emissions at La Soufrière past eruptions.

### 5.2.2 Climate forcing from La Soufrière de Guadeloupe eruptions

Sulphur is considered the most important volatile emitted during eruptions in terms of its climatic impact (Emiliani, 1966; Van Donk, 1976; Marshall et al., 2022). Accordingly, we quantify the climate forcing from the studied eruptions using the EVA\_H simple volcanic aerosol forcing model (Aubry et al., 2020; also see section 3). The eruption latitude is simply specified at that of La Soufrière (16.04°N). The other two critical inputs to EVA\_H are the  $SO_2$  mass and injection altitude, with the  $SO_2$  mass distributed vertically following a Gaussian profile centered on the injection altitude and a width of 1.2 km.

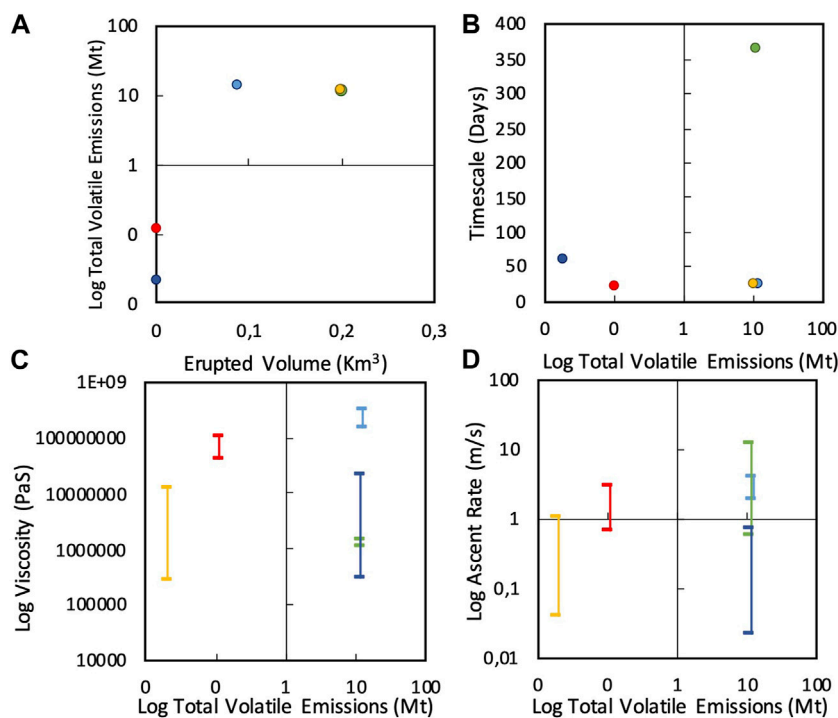


FIGURE 7

(A) Total Volatile Emissions (Mt) vs. VEI; (B) Expected Timescales; (C) Groundmass Viscosity; (D) Ascent Rate vs. Total Volatile Emissions (Mt) for the 1657 CE (red), 1530 CE (light blue), 1010 CE (green), 341 (dark blue) and 5680 BCE (yellow) eruptions. The 1530 CE eruption is an outlier due to the high H<sub>2</sub>O value used which was calculated by difference by Pichavant et al. (2018).

We use the SO<sub>2</sub> mass in Mt calculated using the petrologic method and assume all sulphur is released as SO<sub>2</sub>. Despite the occurrence of H<sub>2</sub>S in the present-day hydrothermal system (e.g., Moune et al., 2022) we assume during a magmatic eruption SO<sub>2</sub> would dominate over any hydrothermal H<sub>2</sub>S input, due to higher temperatures which favour SO<sub>2</sub>. We chose to run scenarios for both the best estimate and the maximum estimate of SO<sub>2</sub> based on the calculated errors. However, as the petrologic method only provides a minimum estimate of volatile emissions, the magnitude of the resulting impact on the climate might be representative of a minimum estimate.

Plume heights above sea level were estimated by Komorowski et al. (2008), Legendre (2012), Esposti Ongaro et al. (2020) and Komorowski et al. (2022) using each eruption isopleth maps (Carey and Sparks, 1986), with a large uncertainty given the scarcity of outcrops (Table 1). The upper estimate of the 1657 CE and 341 CE eruption columns are 15 km a.s.l., which indicates sulphur may not have reached the stratosphere (tropopause altitude in Guadeloupe: 16.58 km; Komorowski et al., 2008) when considering plume heights lower than this upper limit. The Plinian eruption (1010 CE and 5680 BCE) columns are more likely to have reached the stratosphere with plume heights estimated at 10–25 km a.s.l.

As a very large range of plume heights are estimated for La Soufrière, we performed a sensitivity study and modelled SO<sub>2</sub> injections at several altitudes, depending on the eruption. For the VEI two to three eruptions (Table 1), we use SO<sub>2</sub> injection altitude between 10–15 km a.s.l. Given the recent re-evaluation of the maximum plume height for the 1530 CE Sub-Plinian eruption

(16–18 km a.s.l.; Esposti-Ongaro et al., 2020), we also included a scenario with a 17 km a.s.l. SO<sub>2</sub> injection altitude, just above the tropopause. For the VEI 4 eruptions, we tested SO<sub>2</sub> injection altitudes of 10–25 km a.s.l.

Using the SO<sub>2</sub> injection source parameter discussed above (latitude, mass and altitude), we ran the EVA\_H model to calculate SAOD perturbation at 550 nm following each eruption. The modelled global mean SAOD time series show a steep rise over 6–9 months following each eruption, followed by a gradual decay over 1–2 years to a peak followed by a more gradual decay (Figure 9). For the 1657 CE, 1530 CE and 341 CE eruptions, the tropospheric or tropopause-level SO<sub>2</sub> injection altitude and small mass of SO<sub>2</sub> result in negligible peak global mean SAOD perturbation (<0.005; for comparison global mean SAOD peaked around 0.11 after the Pinatubo 1991 eruption). The corresponding global mean effective radiative forcing for the 1530 CE and 1657 CE eruptions and for the 17 km injection scenario is between and –0.00017 to –0.00010 W/m<sup>2</sup>; in comparison effective radiative forcing (ERF) from the 341 CE eruption is much lower, between and –0.000004 and –0.00001 W/m<sup>2</sup>.

In comparison to the smaller VEI two to three eruptions, the 1010 CE and 5680 BCE Plinian eruptions (VEI 4) exert a larger forcing effect. For the 1010 CE eruption, which is considered the smaller of the two Plinian eruptions (Legendre, 2012), and for the 25 km injection scenario, the resulting peak global mean SAOD is 0.0054–0.0055 (Figure 9) and peak global mean ERF is between –0.026 and –0.029 W/m<sup>2</sup>. The 5680 BCE Plinian eruption records the greatest climate forcing with peak global

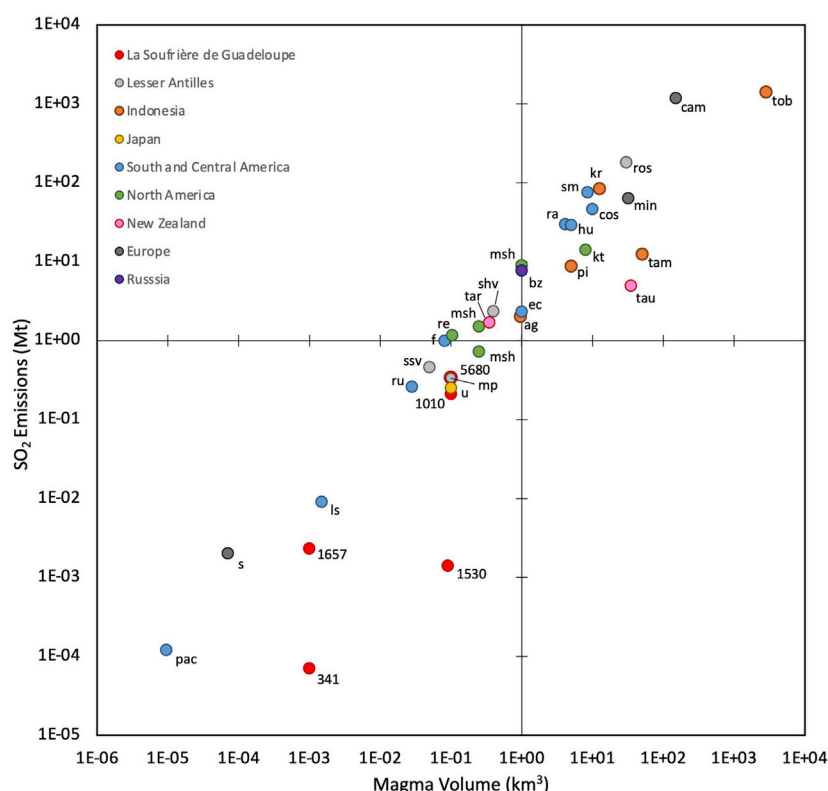


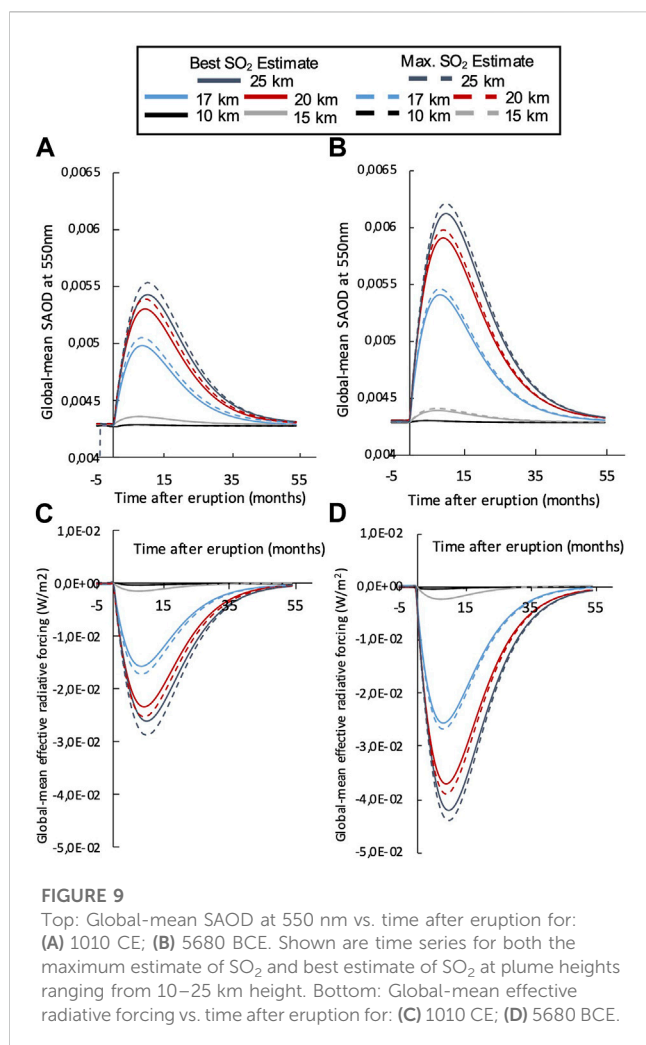
**FIGURE 8**

SO<sub>2</sub> emissions for subduction zone volcanoes calculated from the petrologic method after Wallace, 2003; 2005 and Scaillet et al., 2003. Emissions calculated for this study fit within the global trend, with the 5,680 Cal. BCE and 1,010 Cal. CE eruptions having volumes and emissions comparable to Montagne Pelée and Soufrière St Vincent in the Lesser Antilles. The 341 Cal. CE eruption is outside of the trend, suggesting SO<sub>2</sub> emissions have been underestimated or magma volume has been over estimated. Agung 1963 (ag; Self and King 1996); Samalas 1257 CE. (sa; Vidal et al., 2016); Krakatau 1885 (kr; Mandeville et al., 1998); Pinatubo 1991 (pi; Westrich and Gerlach, 1992); Toba 71000 BP (tob; Scaillet et al., 1998; Zielinski et al., 1996b); Tambora 1815 (tam; Devine et al., 1984; Scaillet et al., 1998); La Soufrière de Guadeloupe 1657 CE (1,657); La Soufrière de Guadeloupe 1,010 Cal. CE (1,010); La Soufrière de Guadeloupe 341 CE (341); La Soufrière de Guadeloupe 5680 BCE (5,680); Montserrat 1995 (shv; Scaillet and Pichavant, 2003); Mont Pelée 1902 (mp; Scaillet et al., 2003); Roseau Tuff 28000 BP (ros; Devine et al., 1984); Soufrière St Vincent 1979 (ssv; Devine et al., 1984; Devine and Sigurdsson, 1983); Unzen 1991 (u; Scaillet and Pichavant, 2003); Shinmoedake 2011 (shi; Mori and Kato 2013); Santa Maria 1902 (sm; Palais and Sigurdsson, 1989; Rose, 1987); Pacaya 1972 (pac; Andres et al., 1991); Fuego 1974 (f; Rose et al., 1984; Roggensack et al., 1997); El Chichon 1982 (ec; Devine et al., 1984; Carey and Sigurdsson, 1986; Krueger et al., 1995; Luhr et al., 1984); Ruiz 1985 (ru; Sigurdsson et al., 1990b); Lascar 1989 (ls; Andres et al., 1991; Matthews et al., 1999); Rabaul (ra; Palais and Sigurdsson, 1989); Coseguina 1835 (cos; Palais and Sigurdsson, 1989); Huaynaputina (hu; Costa et al., 2003); Mount St Helen's 1980, 1800, 1,480 (msh; Gerlach and McGee, 1994; Palais and Sigurdsson, 1989); Bezymianny 1956 (bz; Palais and Sigurdsson, 1989; Zielinski, 1995); Redoubt 1989–91 (re; Gerlach and McGee, 1994; Nye et al., 1994); Katmai 1912 (kt; Westrich et al., 1991); Minoan 3650 BP (min; Devine et al., 1984; Sigurdsson et al., 1990a); Campanian (cam; Palais and Sigurdsson, 1989; Civetta et al., 1997); Stromboli 1980–93 (s; Allard et al., 2014); Tarawera 1886 (tar; Palais and Sigurdsson, 1989); Taupo 181 Cal. CE. (tau; Palais and Sigurdsson, 1989).

mean SAOD ranging between 0.0061 and 0.0062, and peak global mean ERF between  $-0.042$  and  $-0.044$  W/m<sup>2</sup> (Figure 9). As with the smaller eruptions, no significant change from the background level is recorded for plumes not reaching the stratosphere (<15 km). As the plume heights represent an upper estimate of the SO<sub>2</sub> injection height, the forcing effect could be considered an upper bound estimate; however, as the petrologic method underestimates the SO<sub>2</sub> mass injected, this results in a competing effect between the overestimated SO<sub>2</sub> injection height and the underestimated SO<sub>2</sub> mass.

To put the climatic forcing and impact of the studied eruption in perspective, we use the Volcano-Climate Index (VCI) proposed by Schmidt and Black (2022). The main criteria for VCI are decreases in surface temperatures after an eruption, and the scale ranges from VCI 0 (negligible climate effects) to VCI 6+ (long-lasting or even catastrophic global disruption). As an example, the 1991 Mount

Pinatubo (VEI 6; 10 and 20 Tg of SO<sub>2</sub>; 25 km SO<sub>2</sub> injection height; Guo et al., 2004; Read et al., 1993; Carn et al., 2016), resulted in peak local mean SAOD, ERF and surface cooling of 0.1 (Thomason et al., 2021),  $-3$  W/m<sup>2</sup> (Schmidt et al., 2018) and  $-0.5^{\circ}\text{C}$  (McCormick et al., 1995) has a VCI of 3 (Schmidt and Black, 2022). In comparison, based on our obtained SAOD values, all eruptions studied are expected to have VCI 0–1 (negligible climate effects to local and regional climate effects) and are very unlikely to have had any significant footprint on global climate as individual events. However, the reconstructed plume height (upper tropospheric–lower stratospheric), SO<sub>2</sub> mass (on the order of 0.1 to 1 Tg SO<sub>2</sub>) and SAOD perturbation (0.005–0.006) means that they are the type of events typically contributing to the “background stratospheric aerosol layer” variability (Solomon et al., 2011). This variability is governed by relatively moderate-magnitude volcanic events (like the 1010 CE and 5680 BCE La Soufriere



eruptions), but which occur on a multi-annual basis globally and collectively result in significant radiative forcing (e.g., Solomon et al., 2011; Schmidt et al., 2018) and impacts on large-scale climate metrics, including surface cooling (e.g., Santer et al., 2015) and Antarctic ozone hole healing (e.g., Solomon et al., 2016).

## 6 Conclusion

Using new analyses of melt inclusions, we have investigated the volatile life cycle for five eruptions of La Soufrière de Guadeloupe. We report maximum volatile concentrations in the melt inclusions across the five eruptions as: 4.42 wt% H<sub>2</sub>O, 1700 CO<sub>2</sub> ppm, 780 ppm S, 0.36 wt% Cl and 680 ppm F. Our data show a systematic decrease in S over time which indicates the whole system is evolving by separating FeS, which results in a decrease in S content from the oldest magma suite to the youngest. The changes related to decompression degassing and sulphide separation result in a decrease in  $fO_2$  to more reduced conditions in the shallow system.

We also quantify the total volatile emissions using the petrologic method, with the 1010 CE and 5680 BCE eruptions having the highest total volatile emissions (11.6 Mt and 11.3 Mt, respectively),

while the 1657 CE and 341 CE eruptions have considerably lower total emissions at 0.1 and 0.02 Mt, respectively. The 1530 CE eruption has a higher total emission (12.8 Mt), due to the high H<sub>2</sub>O content reported for this eruption (Pichavant et al., 2018). Though the petrologic method underestimates volatile emissions, we show that SO<sub>2</sub> emissions from the 1010 CE and 5680 BCE eruptions are 0.2 Mt and 0.3 Mt of SO<sub>2</sub>, respectively.

Using the calculated SO<sub>2</sub> emissions and plume height constrained from isopleth data, we estimate that the two Plinian eruptions in 1010 CE and 5680 BCE were associated with peak global mean SAOD of 0.0055–0.0062, and peak global mean effective radiative forcing of  $-0.022$  to  $-0.035$  W/m<sup>2</sup> (VCI 0–1). They were therefore, unlikely to exert significant climate disruption but contributed to the stratospheric volcanic aerosol “background” (Solomon et al., 2011). The other smaller La Soufrière de Guadeloupe eruptions investigated exerted negligible climate forcing owing to minor SO<sub>2</sub> masses and tropospheric plume heights.

Overall, this study increases our understanding of La Soufrière de Guadeloupe by providing insights into the volatile processes occurring at depth, such as sulphide separation and sulphur degassing with decompression. Documenting the change in oxidation state in future efforts aimed at modelling the La Soufrière system is a major issue for understanding deep magma evolution and for the purposes of volcanic surveillance. We also provide new insights into the climate forcing effect of volatiles from La Soufrière de Guadeloupe eruptions. This will bring new constraints on the volatile processes occurring at depth and climate forcing effects of VEI two to four eruptions of basaltic-andesitic, magmatic-hydrothermal systems.

## Data availability statement

The original contributions presented in the study are included in the article/Supplementary Material, further inquiries can be directed to the corresponding author.

## Author contributions

AM prepared the samples, acquired the geochemical and petrological data, processed and analysed the data. RM and AM ran the CHOSETTO models, discussed and interpreted the data. TA ran the EVA\_H models and with AM discussed and interpreted the data. J-CK, SM, and AM undertook fieldwork and sampling. AM drafted the manuscript and figures. All authors contributed to the article and approved the submitted version.

## Funding

This work was supported by the Institut National des Sciences de l’Univers (INSU-CNRS) for radiocarbon dating (AO Artemis, LMC14-CEA Saclay), and the CASAVA Project funded by Agence Nationale de la Recherche, 2009–2015 (ANR-09-RISK-02). The PhD scholarship of AM was co-funded by the “Make our Planet Great Again” initiative (Campus France) and the IPGP Ecole Doctorale. We thank IPGP for general funding to the Observatoires Volcanologiques

et Sismologiques (OVS), the INSU-CNRS for funding provided to the Service National d'Observation en Volcanologie (SNOV), a INSU-CNRS Tellus-Aleas project to SM (2020, Insights into the dynamics of the active hydrothermal system of La Soufrière de Guadeloupe from past eruptions), and the Ministère pour la Transition Ecologique et Solidaire (MTES) for financial support. This work has been supported by the Clervolc (UCA-LMV), the AO-IPGP 2018 project “Depth to surface propagation of fluid-related anomalies at La Soufrière de Guadeloupe volcano (FWI): timing and implications for volcanic unrest” (coord.: MR), the project “Vers la Plateforme Régionale de Surveillance Tellurique du futur” (PREST) co-funded by INTERREG Caraïbes V for the European Regional Development Fund, and the European Union’s Horizon 2020 research and innovation programme, under grant agreement No 731070 (EUROVOLC project). TA acknowledges support from the Cambridge Sidney Sussex College through a Junior Research Fellowship during completion of this work.

## Acknowledgments

The authors thank the OVSG-IPGP team for logistical support and help with data collection. We are grateful for help and information from Laurence and E. Barret (Vert Intense). We thank Y. Legendre for assistance in the field and discussions of the geology and the eruptive past reconstruction of La Soufrière. We are grateful to the Parc National de Guadeloupe for allowing us to undertake research and obtain geological samples. Radiocarbon dates were obtained from Beta Analytical. TJA acknowledges support from the Cambridge Sidney

Sussex College through a Junior Research Fellowship during completion of this work. Finally, we would like to thank the two reviewers. This study contributes to the IdEx Université de Paris ANR-18-IDEX-0001 and is Laboratory of excellence ClerVolc contribution number 604.

## Conflict of interest

The authors declare that the research was conducted in the absence of any commercial or financial relationships that could be construed as a potential conflict of interest.

## Publisher’s note

All claims expressed in this article are solely those of the authors and do not necessarily represent those of their affiliated organizations, or those of the publisher, the editors and the reviewers. Any product that may be evaluated in this article, or claim that may be made by its manufacturer, is not guaranteed or endorsed by the publisher.

## Supplementary material

The Supplementary Material for this article can be found online at: <https://www.frontiersin.org/articles/10.3389/feart.2023.1143325/full#supplementary-material>

## References

- Aiuppa, A., Bertagnini, A., Métrich, N., Moretti, R., Di Muro, A., Liuzzo, M., et al. (2010). A model of degassing for Stromboli volcano. *Earth Planet. Sci. Lett.* 295 (1-2), 195–204. doi:10.1016/j.epsl.2010.03.040
- Aiuppa, A., Bitetto, M., Calabrese, S., Delle Donne, D., Lages, J., La Monica, F. P., et al. (2022). Mafic magma feeds degassing unrest at Vulcano Island, Italy. *Commun. Earth Environ.* 3 (1), 255–315. doi:10.1038/s43247-022-00589-1
- Aiuppa, A., Fischer, T. P., Plank, T., Robidoux, P., and Di Napoli, R. (2017). Along-arc, inter-arc and arc-to-arc variations in volcanic gas CO<sub>2</sub>/ST ratios reveal dual source of carbon in arc volcanism. *Earth-Science Rev.* 168, 24–47. doi:10.1016/j.earscirev.2017.03.005
- Aiuppa, A., Moretti, R., Federico, C., Giudice, G., Gurrieri, S., Liuzzo, M., et al. (2007). Forecasting Etna eruptions by real-time observation of volcanic gas composition. *Geology* 35 (12), 1115–1118. doi:10.1130/g24149a.1
- Allard, P., Aiuppa, A., Beauce, F., Gaudin, D., Di Napoli, R., Calabrese, S., et al. (2014). Steam and gas emission rate from La Soufrière volcano, Guadeloupe (lesser Antilles): Implications for the magmatic supply during degassing unrest. *Chem. Geol.* 384, 76–93. doi:10.1016/j.chemgeo.2014.06.019
- Anderson, A. T., and Wright, T. L. (1972). Phenocrysts and glass inclusions and their bearing on oxidation and mixing of basaltic magmas, Kilauea volcano, Hawaii. *Am. Mineralogist J. Earth Planet. Mater.* 57 (1-2), 188–216.
- Andres, R. J., Rose, W. L., Kyle, P. R., DeSilva, S., Francis, P., Gardeweg, M., et al. (1991). Excessive sulfur dioxide emissions from Chilean volcanoes. *J. Volcanol. Geotherm. Res.* 46 (3-4), 323–329. doi:10.1016/0377-0273(91)90091-d
- Annen, C., Blundy, J. D., and Sparks, R. S. J. (2006). The Genesis of intermediate and silicic magmas in deep crustal hot zones. *J. Petrology* 47 (3), 505–539. doi:10.1093/ptrology/legi084
- Aubry, T. J., Toohey, M., Marshall, L., Schmidt, A., and Jellinek, A. M. (2020). A new volcanic stratospheric sulfate aerosol forcing emulator (EVA\_H): Comparison with interactive stratospheric aerosol models. *J. Geophys. Res. Atmos.* 125 (3), e2019JD031303. doi:10.1029/2019jd031303
- Bachmann, O., and Bergantz, G. W. (2006). Gas percolation in upper-crustal silicic crystal mushes as a mechanism for upward heat advection and rejuvenation of near-solidus magma bodies. *J. Volcanol. Geotherm. Res.* 149 (1-2), 85–102. doi:10.1016/j.jvolgeores.2005.06.002
- Balcone-Boissard, H., Villemant, B., and Boudon, G. (2010). Behavior of halogens during the degassing of felsic magmas. *Geochem. Geophys. Geosystems* 11 (9), Q09005. doi:10.1029/2010gc003028
- Barnoud, A., Coutant, O., Bouligand, C., Gunawan, H., and Deroussi, S. (2016). 3-D linear inversion of gravity data: Method and application to basse-terre volcanic island, Guadeloupe, lesser Antilles. *Geophys. Suppl. Mon. Notices R. Astronomical Soc.* 205 (1), 562–574. doi:10.1093/gji/ggw030
- Blundy, J., Cashman, K. V., Rust, A., and Witham, F. (2010). A case for CO<sub>2</sub>-rich arc magmas. *Earth Planet. Sci. Lett.* 290, 289–301. doi:10.1016/j.epsl.2009.12.013
- Blundy, J., and Cashman, K. (2008). Petrologic reconstruction of magmatic system variables and processes. *Rev. Mineralogy Geochem.* 69 (1), 179–239. doi:10.2138/rmg2008.69.6
- Botcharnikov, R. E., Koepke, J., Holtz, F., McCammon, C., and Wilke, M. (2005). The effect of water activity on the oxidation and structural state of Fe in a ferro-basaltic melt. *Geochim. Cosmochimica Acta* 69, 5071–5085. doi:10.1016/j.gca.2005.04.023
- Boudon, G., Dagain, J., Semet, M. P., and Westercamp, D. (1988). *Notice explicative de la carte géologique au 1/20.000 ème du massif volcanique de la Soufrière (Département de la Guadeloupe, Petites Antilles)*. Paris: BRGM, CNRS, DRM, IPGP, 43.
- Boudon, G., Komorowski, J. C., Villemant, B., and Semet, M. P. (2008). A new scenario for the last magmatic eruption of La Soufrière de Guadeloupe (Lesser Antilles) in 1530 AD: Evidence from stratigraphy radiocarbon dating and magmatic evolution of erupted products. *J. Volcanol. Geotherm. Res.* 178 (3), 474–490. doi:10.1016/j.jvolgeores.2008.03.006
- Boudon, G., Le Friant, A., Komorowski, J. C., Deplus, C., and Semet, M. P. (2007). Volcano flank instability in the Lesser Antilles Arc: Diversity of scale, processes, and temporal recurrence. *J. Geophys. Res. Solid Earth* 112 (8), B08205. doi:10.1029/2006jb004674
- Brombach, T., Marini, L., and Hunziker, J. C. (2000). Geochemistry of the thermal springs and fumaroles of basse-terre island, Guadeloupe, lesser Antilles. *Bull. Volcanol.* 61, 477–490. doi:10.1007/pl00008913
- Bronce, M., Stolper, E., and Eiler, J. (2017). Redox variations in Mauna Kea lavas, the oxygen fugacity of the Hawaiian plume, and the role of volcanic gases in Earth’s oxygenation. *Proc. Natl. Acad. Sci.* 114 (34), 8997–9002. doi:10.1073/pnas.1619527114

- Burgisser, A., and Scaillet, B. (2007). Redox evolution of a degassing magma rising to the surface. *Nature* 445 (7124), 194–197. doi:10.1038/nature05509
- Cabrera, A., Weinberg, R. F., Wright, H. M., Zlotnik, S., and Cas, R. A. (2011). Melt fracturing and healing: A mechanism for degassing and origin of silicic obsidian. *Geology* 39 (1), 67–70. doi:10.1130/g31355.1
- Candela, P. A. (1986). The evolution of aqueous vapor from silicate melts: Effect on oxygen fugacity. *Geochimica Cosmochimica Acta* 50 (6), 1205–1211. doi:10.1016/0016-7037(86)90403-5
- Carey, S., and Sparks, R. S. J. (1986). Quantitative models of the fallout and dispersal of tephra from volcanic eruption columns. *Bull. Volcanol.* 48, 109–125.
- Caricchi, L., Sheldrake, T. E., and Blundy, J. (2018). Modulation of magmatic processes by CO<sub>2</sub> flushing. *Earth Planet. Sci. Lett.* 491, 160–171. doi:10.1016/j.epsl.2018.03.042
- Carlsen, H. K., Ilyinskaya, E., Baxter, P. J., Schmidt, A., Thorsteinsson, T., Pfeffer, M. A., et al. (2021). Increased respiratory morbidity associated with exposure to a mature volcanic plume from a large Icelandic fissure eruption. *Nat. Commun.* 12 (1), 2161–2212. doi:10.1038/s41467-021-22432-5
- Carmichael, I. S., and Ghiorso, M. S. (1986). Oxidation-reduction relations in basic magma: A case for homogeneous equilibria. *Earth Planet. Sci. Lett.* 78, 200–210. doi:10.1016/0012-821x(86)90061-0
- Carn, S. A., Clarisse, L., and Prata, A. J. (2016). Multi-decadal satellite measurements of global volcanic degassing. *J. Volcanol. Geotherm. Res.* 311, 99–134. doi:10.1016/j.jvolgeores.2016.01.002
- Carroll, M. R., and Rutherford, M. J. (1985). Sulfide and sulfate saturation in hydrous silicate melts. *J. Geophys. Res. Solid Earth* 90 (S02), C601–C612. doi:10.1029/jb090is02p0c601
- Cashman, K. V., Sparks, R. S. J., and Blundy, J. D. (2017). Vertically extensive and unstable magmatic systems: A unified view of igneous processes. *Science* 355 (6331), eaag3055. doi:10.1126/science.aag3055
- Cassidy, M., Manga, M., Cashman, K., and Bachmann, O. (2018). Controls on explosive-effusive volcanic eruption styles. *Nat. Commun.* 9 (1), 2839. doi:10.1038/s41467-018-05293-3
- Castro, J. M., Burgisser, A., Schipper, C. I., and Mancini, S. (2012). Mechanisms of bubble coalescence in silicic magmas. *Bull. Volcanol.* 74 (10), 2339–2352. doi:10.1007/s00445-012-0666-1
- Cicconi, M. R., Le Losq, C., Moretti, R., and Neuville, D. R. (2020). Magmas are the largest repositories and carriers of earth's redox processes. *Elements* 16 (3), 173–178. doi:10.2138/elements.16.3.173
- Collins, S. J., MacLennan, J., Pyle, D. M., Barnes, S. J., and Upton, B. G. J. (2012). Two phases of sulphide saturation in Réunion magmas: Evidence from cumulates. *Earth Planet. Sci. Lett.* 337, 104–113. doi:10.1016/j.epsl.2012.05.027
- Davidson, P., and Kamenetsky, V. S. (2007). Primary aqueous fluids in rhyolitic magmas: Melt inclusion evidence for pre- and post-trapping exsolution. *Chem. Geol.* 237 (3–4), 372–383. doi:10.1016/j.chemgeo.2006.07.009
- de Moor, J. M., Aiuppa, A., Pacheco, J., Avaró, G., Kern, C., Liuzzo, M., et al. (2016). Short-range volcanic gas precursors to phreatic eruptions: Insights from Poás Volcano, Costa Rica. *Earth Planet. Sci. Lett.* 442, 218–227. doi:10.1016/j.epsl.2016.02.056
- DeMets, C., Jansma, P. E., Mattioli, G. S., Dixon, T. H., Farina, F., Bilham, R., et al. (2000). GPS geodetic constraints on Caribbean-North America plate motion. *Geophys. Res. Lett.* 27 (3), 437–440. doi:10.1029/1999gl005436
- Deng, J., and Sykes, L. R. (1995). Determination of Euler pole for contemporary relative motion of Caribbean and North American plates using slip vectors of interplate earthquakes. *Tectonics* 14 (1), 39–53. doi:10.1029/94tc02547
- Devine, J. D., Sigurdsson, H., Davis, A. N., and Self, S. (1984). Estimates of sulfur and chlorine yield to the atmosphere from volcanic eruptions and potential climatic effects. *J. Geophys. Res. Solid Earth* 89 (B7), 6309–6325.
- Dixon, T. H., Farina, F., DeMets, C., Jansma, P., Mann, P., and Calais, E. (1998). Relative motion between the Caribbean and North American plates and related boundary zone deformation from a decade of GPS observations. *J. Geophys. Res. Solid Earth* 103 (7), 15157–15182. doi:10.1029/97jb03575
- Edmonds, M., and Herd, R. A. (2007). A volcanic degassing event at the explosive-effusive transition. *Geophys. Res. Lett.* 34 (21), L21310. doi:10.1029/2007gl031379
- Edmonds, M., and Mather, T. A. (2017). Volcanic sulfides and outgassing. *Elements* 13 (2), 105–110. doi:10.2113/elements.13.2.105
- Edmonds, M., and Wallace, P. J. (2017). Volatiles and exsolved vapor in volcanic systems. *Elements* 13 (1), 29–34. doi:10.2113/elements.13.1.29
- Eichelberger, J. C., Carrigan, C. R., Westrich, H. R., and Price, R. H. (1986). Non-explosive silicic volcanism. *Nature* 323 (6089), 598–602. doi:10.1038/323598a0
- Emiliani, C. (1966). Paleotemperature analysis of Caribbean cores P6304-8 and P6304-9 and a generalized temperature curve for the past 425,000 years. *J. Geol.* 74 (2), 109–124. doi:10.1086/627150
- Esposito Ongaro, T., Komorowski, J.-C., Legendre, Y., and Neri, A. (2020). Modelling pyroclastic density currents from a subplinian eruption at La Soufrière de Guadeloupe (West Indies, France). *Bull. Volcanol.* 82, 76. doi:10.1007/s00445-020-01411-6
- Feuillet, N., Beauducel, F., and Tapponnier, P. (2011). Tectonic context of moderate to large historical earthquakes in the Lesser Antilles and mechanical coupling with volcanoes. *J. Geophys. Res.* 116, B10308. doi:10.1029/2011JB008443
- Feuillard, M., Allègre, C. J., Brandeis, G., Gaulon, R., Le Mouél, J. L., Mercier, J. C., et al. (1983). The 1975–1977 crisis of La Soufrière de Guadeloupe (FWI): A still-born magmatic eruption. *J. Volcanol. Geotherm. Res.* 16 (3–4), 317–334. doi:10.1016/0377-0273(83)90036-7
- Gaillard, F., Scaillet, B., and Arndt, N. T. (2011). Atmospheric oxygenation caused by a change in volcanic degassing pressure. *Nature* 478 (7368), 229–232. doi:10.1038/nature10460
- Gaillard, F., Scaillet, B., Pichavant, M., and Iacono-Marziano, G. (2015). The redox geodynamics linking basalts and their mantle sources through space and time. *Chem. Geol.* 418, 217–233. doi:10.1016/j.chemgeo.2015.07.030
- Gennaro, E., Paonita, A., Iacono-Marziano, G., Moussallam, Y., Pichavant, M., Peters, N., et al. (2020). Sulphur behaviour and redox conditions in etnean magmas during magma differentiation and degassing. *J. Petrology* 61 (10), ega095. doi:10.1093/petrology/egaa095
- Gerlach, T. M., and McGee, K. A. (1994). Total sulfur dioxide emissions and pre-eruption vapor-saturated magma at Mount St. Helens, 1980–88. *Geophys. Res. Lett.* 21 (25), 2833–2836. doi:10.1029/94gl02761
- Gerlach, T. M., Westrich, H. R., and Symonds, R. B. (1996). Preeruption vapor in magma of the climactic Mount Pinatubo eruption: Source of the giant stratospheric sulfur dioxide cloud. *Fire mud eruptions lahars Mt. Pinatubo Philipp.* 415, 33.
- Giggenbach, W. F. (1988). Geothermal solute equilibria. Derivation of Na-K-Mg-Ca geothermometers. *Geochim. Cosmochim. Acta* 52, 2749–2765. doi:10.1016/0016-7037(88)90143-3
- Giggenbach, W. F. (1997). “The origin and evolution of fluids in magmatic-hydrothermal systems,” in *Geochemistry of hydrothermal ore deposits*. Editor H. L. Barnes 3d Edition (Hoboken, NJ: Wiley), 737–796.
- Gonnermann, H. M., and Manga, M. (2003). Explosive volcanism may not be an inevitable consequence of magma fragmentation. *Nature* 426 (6965), 432–435. doi:10.1038/nature02138
- Graf, H. F., Feichter, J., and Langmann, B. (1997). Volcanic sulfur emissions: Estimates of source strength and its contribution to the global sulfate distribution. *J. Geophys. Res. Atmos.* 102 (9), 10727–10738. doi:10.1029/96jd03265
- Guo, S., Bluth, G. J. S., Rose, W. I., Watson, I. M., and Prata, A. J. (2004). Re-evaluation of SO<sub>2</sub> release of the 15 June 1991 Pinatubo eruption using ultraviolet and infrared satellite sensors. *Geochem Geophys Geosyst* 5 (4), Q04001. doi:10.1029/2003gc000654
- Gurenko, A. A., Belousov, A. B., Trumbull, R. B., and Sobolev, A. V. (2005). Explosive basaltic volcanism of the Chikurachki Volcano (Kurile arc, Russia): insights on pre-eruptive magmatic conditions and volatile budget revealed from phenocryst-hosted melt inclusions and groundmass glasses. *J. Volcanol. Geotherm. Res.* 147 (3–4), 203–232.
- Hauri, E. (2002). SIMS analysis of volatiles in silicate glasses, 2: Isotopes and abundances in Hawaiian melt inclusions. *Chem. Geol.* 183 (1–4), 115–141. doi:10.1016/s0009-2541(01)00374-6
- Hedenquist, J. W., and Lowenstern, J. B. (1994). The role of magmas in the formation of hydrothermal ore deposits. *Nature* 370, 519–527. doi:10.1038/370519a0
- Hincks, T. K., Komorowski, J. C., Sparks, S. R., and Aspinall, W. P. (2014). Retrospective analysis of uncertain eruption precursors at La soufrière volcano, Guadeloupe, 1975–77: Volcanic hazard assessment using a bayesian belief network approach. *J. Appl. Volcanol.* 3 (1), 3–26. doi:10.1186/2191-5040-3-3
- Huber, C., Bachmann, O., and Dufek, J. (2011). Thermo-mechanical reactivation of locked crystal mushes: Melting-induced internal fracturing and assimilation processes in magmas. *Earth Planet. Sci. Lett.* 304 (3–4), 443–454. doi:10.1016/j.epsl.2011.02.022
- Hughes, E. C., Saper, L., Liggins, P., O'Neill, H. S. C., and Stolper, E. M. (2022). The sulfur solubility minimum and maximum in silicate melt. *J. Geol. Soc.* 180 (3), jgs2021–125. doi:10.1144/jgs2021-125
- Inostroza, M., Moune, S., Moretti, R., Bonifacie, M., Robert, V., Burtin, A., et al. (2022a). Decoding water-rock interaction and volatile input at La Soufrière volcano (Guadeloupe) using time-series major and trace element analyses in gas condensates. *J. Volcanol. Geotherm. Res.* 425, 107517. doi:10.1016/j.jvolgeores.2022.107517
- Inostroza, M., Moune, S., Moretti, R., Robert, V., Bonifacie, M., Chilin-Eusebe, E., et al. (2022b). Monitoring Hydrothermal Activity Using Major and Trace Elements in Low-Temperature Fumarolic Condensates: The Case of La Soufrière de Guadeloupe Volcano. *Geosciences* 12 (7), 267. doi:10.3390/geosciences12070267
- Jarrard, R. D. (1986). Relations among subduction parameters. *Rev. Geophys.* 24 (2), 217–284. doi:10.1029/rg024i002p0217
- Jenner, F. E. (2017). Cumulate causes for the low contents of sulfide-loving elements in the continental crust. *Nat. Geosci.* 10 (7), 524–529. doi:10.1038/ngeo2965
- Jessop, D. E., Moune, S., Moretti, R., Gibert, D., Komorowski, J. C., Robert, V., et al. (2021). A multi-decadal view of the heat and mass budget of a volcano in unrest: La Soufrière de Guadeloupe (French west indies). *Bull. Volcanol.* 83, 16–19. doi:10.1007/s00445-021-01439-2
- Kelley, K. A., and Cottrell, E. (2012). The influence of magmatic differentiation on the oxidation state of Fe in a basaltic arc magma. *Earth Planet. Sci. Lett.* 329, 109–121. doi:10.1016/j.epsl.2012.02.010

- Kelley, K. A., and Cottrell, E. (2009). Water and the oxidation state of subduction zone magmas. *Science* 325 (5940), 605–607. doi:10.1126/science.1174156
- Kilgour, G., Moune, S., Della Pasqua, F., and Christenson, B. (2016). “Petrological insights into the 1976–2000 eruption episode of white island, New Zealand: An eruption fuelled by repeated mafic recharge,” in EGU General Assembly Conference Abstracts, Vienna, Austria, April 17–22, 2016, EPSC2016–13528.
- Komorowski, J.-C., Legendre, Y., and Barsotti, S. (2013). “Assessing long term hazards for La soufrière de Guadeloupe volcano: Insights from a new eruptive chronology, credible scenario definition, and integrated impact modelling,” in International Association of Volcanology and Chemistry of the Earth’s Interior (IAVCEI), Scientific Assembly, Kagoshima, Japan, July 19–24, 2013.
- Komorowski, J.-C., Legendre, Y., and Boudon, G. (2012). “A new Holocene eruptive chronology for La soufrière de Guadeloupe volcano: Implications for credible scenario definition as well as hazard and impact modelling,” in International Association of Volcanology and Chemistry of the Earth’s Interior (IAVCEI), Cities on Volcanoes 7, Colima, Mexico, November 18–23, 2012.
- Komorowski, J.-C., Legendre, Y., Metcalfe, A., Moretti, R., Moune, S., Rosas-Carbajal, M., et al. (2022). European catalogue of volcanoes. IMO, UI and CPD-NCIP. Available at: <https://volcanos.eurovolc.eu/?volcano=SDG#>.
- Komorowski, J.-C., Boudon, G., Antenor-Habazac, C., Hammouya, G., Semet, M., David, J., et al. (2001). *L’activité éruptive et non-éruptive de La Soufrière de Guadeloupe: Problèmes et implications de la phénoménologie et des signaux actuellement enregistrés (French). Eruptive and non-eruptive activity from La Soufrière de Guadeloupe: Problems and implications posed by the current phenomenology and monitoring signals. Workshop on volcanic hazards - lesser Antilles volcanoes: From processes to signals.* Paris: INSU Lesser Antilles Volcanic Hazard Workshop, 18–19.
- Komorowski, J. C., Boudon, G., Semet, M., Beauducel, F., Antenor-Habazac, C., Bazin, S., et al. (2005). *Volcanic hazard atlas of the lesser Antilles. Seismic research uni.* Trinidad and Tobago, WI: The University of the West Indies, 65–102.
- Komorowski, J. C., Legendre, Y., Caron, B., and Boudon, G. (2008). Reconstruction and analysis of sub-plinian tephra dispersal during the 1530 AD Soufrière (Guadeloupe) eruption: Implications for scenario definition and hazards assessment. *J. Volcanol. Geotherm. Res.* 178 (3), 491–515. doi:10.1016/j.jvolgeoes.2007.11.022
- Kopp, H., Weinzierl, W., Becel, A., Charvis, P., Evain, M., Flueh, E., et al. (2011). Deep structure of the central lesser Antilles island arc: Relevance for the formation of continental crust. *Earth Planet. Sci. Lett.* 304 (1–2), 121–134. doi:10.1016/j.epsl.2011.01.024
- Kyser, T. K., and O’Neil, J. R. (1984). Hydrogen isotope systematics of submarine basalts. *Geochimica Cosmochimica Acta* 48 (10), 2123–2133. doi:10.1016/0016-7037(84)90392-2
- Lee, C. T. A., and Tang, M. (2020). How to make porphyry copper deposits. *Earth Planet. Sci. Lett.* 529, 115868. doi:10.1016/j.epsl.2019.115868
- Legendre, Y. (2012). “Reconstruction fine de l’histoire éruptive et scénarii éruptifs à La Soufrière de Guadeloupe: Vers un modèle intégré de fonctionnement du volcan.” Doctoral dissertation (Paris: Université Paris).
- Lester, G. W., Clark, A. H., Kyser, T. K., and Naslund, H. R. (2013). Experiments on liquid immiscibility in silicate melts with H<sub>2</sub>O, P, S, F and Cl: implications for natural magmas. *Contrib. to Mineral. Petrol.* 166, 329–349.
- Liu, Y., Anderson, A. T., and Wilson, C. J. (2007). Melt pockets in phenocrysts and decompression rates of silicic magmas before fragmentation. *J. Geophys. Res. Solid Earth* 112 (B6), B06204. doi:10.1029/2006jb004500
- Lowenstern, J. B. (1994). Chlorine, fluid immiscibility, and degassing in peralkaline magmas from Pantelleria, Italy. *Am. Mineralogist* 79 (3–4), 353–369.
- Luhr, J. F., Carmichael, I. S., and Varekamp, J. C. (1984). The 1982 eruptions of El Chichón volcano, Chiapas, Mexico: Mineralogy and petrology of the anhydrite-bearing pumices. *J. Volcanol. Geotherm. Res.* 23 (1–2), 69–108. doi:10.1016/0377-0273(84)90057-x
- Macdonald, F. A., and Wordsworth, R. (2017). Initiation of Snowball Earth with volcanic sulfur aerosol emissions. *Geophys. Res. Lett.* 44 (4), 1938–1946. doi:10.1002/2016gl072335
- Macdonald, K. C., and Holcombe, T. L. (1978). Inversion of magnetic anomalies and sea-floor spreading in the Cayman Trough. *Earth Planet. Sci. Lett.* 40 (3), 407–414. doi:10.1016/0012-821x(78)90163-2
- Macdonald, R., Hawkesworth, C. J., and Heath, E. (2000). The lesser Antilles volcanic chain: A study in arc magmatism. *Earth-Science Rev.* 49 (1–4), 1–76. doi:10.1016/s0012-8252(99)00069-0
- Marini, L., Moretti, R., and Accornero, M. (2011). Sulfur isotopes in magmatic-hydrothermal systems, melts, and magmas. *Rev. Mineralogy Geochem.* 73 (1), 423–492. doi:10.2138/rmg.2011.73.14
- Marshall, L., Johnson, J. S., Mann, G. W., Lee, L., Dhoms, S. S., Regayre, L., et al. (2019). Exploring how eruption source parameters affect volcanic radiative forcing using statistical emulation. *J. Geophys. Res. Atmos.* 124 (2), 964–985. doi:10.1029/2018jd028675
- Marshall, L. R., Maters, E. C., Schmidt, A., Timmreck, C., Robock, A., and Toohey, M. (2022). Volcanic effects on climate: Recent advances and future avenues. *Bull. Volcanol.* 84 (5), 54–14. doi:10.1007/s00445-022-01559-3
- McCann, W. R., and Sykes, L. R. (1984). Subduction of aseismic ridges beneath the Caribbean plate: Implications for the tectonics and seismic potential of the northeastern Caribbean. *J. Geophys. Res. Solid Earth* 89 (B6), 4493–4519. doi:10.1029/jb089ib06p04493
- McCormick, M. P., Thomason, L. W., and Trepte, C. R. (1995). Atmospheric effects of the Mt Pinatubo eruption. *Nature* 373 (6513), 399–404. doi:10.1038/373399a0
- Metcalfe, A., Moune, S., Komorowski, J. C., and Moretti, R. (2022). Bottom-up vs top-down drivers of eruption style: Petro-geochemical constraints from the Holocene explosive activity at La Soufrière de Guadeloupe. *J. Volcanol. Geotherm. Res.* 424, 107488. doi:10.1016/j.jvolgeoes.2022.107488
- Metcalfe, A., Moune, S., Komorowski, J.-C., Robertson, R., Christopher, T. E., Joseph, E. J., et al. (2023). A review of the lesser Antilles Arc: What can we learn from magma storage, magma composition and the implications on eruptive style across the arc? *Earth Sci. Rev.* 241, 104440. doi:10.1016/j.earscirev.2023.104440
- Metcalfe, A., Moune, S., Komorowski, J. C., Kilgour, G., Jessop, D. E., Moretti, R., et al. (2021b). *Corrigendum: Magmatic Processes at La Soufrière de Guadeloupe: Insights from Crystal Studies and Diffusion Timescales for eruption onset.* *Front. Earth Sci.* 9, 78. doi:10.3389/feart.2021.723763
- Metcalfe, A., Moune, S., Komorowski, J. C., Kilgour, G., Jessop, D. E., Moretti, R., et al. (2021a). Magmatic Processes at La Soufrière de Guadeloupe: Insights from Crystal Studies and Diffusion Timescales for eruption onset. *Front. Earth Sci.* 9, 78. doi:10.3389/feart.2021.617294
- Métrich, N., and Wallace, P. J. (2008). Volatile abundances in basaltic magmas and their degassing paths tracked by melt inclusions. *Rev. Mineral. Geochem* 69, 363–402. doi:10.2138/rmg.2008.69.10
- Métrich, N., Berry, A. J., O’Neill, H. S. C., and Susini, J. (2009). The oxidation state of sulfur in synthetic and natural glasses determined by X-ray absorption spectroscopy. *Geochimica Cosmochimica Acta* 73 (8), 2382–2399. doi:10.1016/j.gca.2009.01.025
- Métrich, N., and Deloué, E. (2014). Water content,  $\delta D$  and  $\delta^{11}B$  tracking in the Vanuatu arc magmas (Aoba Island): Insights from olivine-hosted melt inclusions. *Lithos* 206, 400–408. doi:10.1016/j.lithos.2014.08.011
- Moretti, R. (2021). “Chapter 6 ionic syntax and equilibrium approach to redox exchanges in melts: Basic concepts and the case of iron and sulfur in degassing magmas,” in *Magma redox geochemistry, geophysical monograph 266*. Editors R. Moretti and D. R. Neuville 1st (Washington, USA: American Geophysical Union).
- Moretti, R., Arienzo, I., Civetta, L., Orsi, G., and D’Antonio, M. (2013a). The deep plumbing system of the ischia island: A physico-chemical window on the fluid-saturated and CO<sub>2</sub>-sustained neapolitan volcanism (southern Italy). *J. Petrology* 54, 951–984. doi:10.1093/ptrology/egt002
- Moretti, R., Arienzo, I., Civetta, L., Orsi, G., and Papale, P. (2013b). Multiple magma degassing sources at an explosive volcano. *Earth Planet. Sci. Lett.* 367, 95–104. doi:10.1016/j.epsl.2013.02.013
- Moretti, R., and Baker, D. R. (2008). Modeling the interplay of fO<sub>2</sub> and fS<sub>2</sub> along the FeS-silicate melt equilibrium. *Chem. Geol.* 256 (3–4), 286–298. doi:10.1016/j.chemgeo.2008.06.055
- Moretti, R., De Natale, G., and Troise, C. (2017). A geochemical and geophysical reappraisal to the significance of the recent unrest at Campi Flegrei caldera (Southern Italy). *Geochem. Geophys. Geosystems* 18 (3), 1244–1269. doi:10.1002/2016gc006569
- Moretti, R., Komorowski, J. C., Ucciani, G., Moune, S., Jessop, D., de Chabalier, J. B., et al. (2020a). The 2018 unrest phase at La Soufrière de Guadeloupe (French West Indies) andesitic volcano: Scrutiny of a failed but prodromal phreatic eruption. *J. Volcanol. Geotherm. Res.* 393, 106769. doi:10.1016/j.jvolgeoes.2020.106769
- Moretti, R., Métrich, N., Arienzo, I., Di Renzo, V., Aiuppa, A., and Allard, P. (2018). Degassing vs. eruptive styles at Mt. Etna volcano (Sicily, Italy). Part I: Volatile stocking, gas fluxing, and the shift from low-energy to highly explosive basaltic eruptions. *Chem. Geol.* 482, 1–17. doi:10.1016/j.chemgeo.2017.09.017
- Moretti, R., Moune, S., Jessop, D., Glynn, C., Robert, V., and Deroussi, S. (2021). The basse-terre island of Guadeloupe (eastern Caribbean, France) and its volcanic-hydrothermal geodiversity: A case study of challenges, perspectives, and new paradigms for resilience and sustainability on volcanic islands. *Geosciences* 11 (11), 454. doi:10.3390/geosciences11110454
- Moretti, R., Moune, S., Robert, V., Jessop, D. E., Didier, T., Bonifacie, M., et al. (2020b). Intercomparison of geochemical techniques at La Soufrière de Guadeloupe (FWI) volcano: Their advantages and their limits over a long-standing unrest. *Italian J. Geosciences* 139 (3), 398–412. doi:10.3301/IJG.2020.13
- Moretti, R., and Ottonello, G. (2003). Polymerization and disproportionation of iron and sulfur in silicate melts: Insights from an optical basicity-based approach. *J. Non-Crystalline Solids* 323 (1–3), 111–119. doi:10.1016/s0022-3093(03)00297-7
- Moretti, R., and Ottonello, G. (2022). Silicate melt thermochemistry and the redox state of magmas. *Rev. Mineralogy Geochem.* 87 (1), 339–403.
- Moretti, R., and Ottonello, G. (2005). Solubility and speciation of sulfur in silicate melts: The Conjugated Toop-Samis-Flood-Grjothelm (CTSFG) model. *Geochimica Cosmochimica Acta* 69 (4), 801–823. doi:10.1016/j.gca.2004.09.006
- Moretti, R., and Papale, P. (2004). On the oxidation state and volatile behavior in multicomponent gas–melt equilibria. *Chem. Geol.* 213 (1–3), 265–280. doi:10.1016/j.chemgeo.2004.08.048

- Moretti, R., Papale, P., and Ottonello, G. (2003). A model for the saturation of COHS fluids in silicate melts. *Geol. Soc. Lond. Spec. Publ.* 213 (1), 81–101.
- Moretti, R. (2005). Polymerisation, basicity, oxidation state and their role in ionic modelling of silicate melts. *Ann. Geophys.* 48 (4). doi:10.4401/ag-3221
- Moretti, R. (2022). Redox behavior of degassing magmas: Critical review and comparison of glass-based oxybarometers with application to Etna volcano. *Comptes Rendus Géoscience* 354 (1), 249–279. doi:10.5802/crgeos.135
- Moretti, R., and Stefánsson, A. (2020). Volcanic and geothermal redox engines. *Elements* 16 (3), 179–184. doi:10.2138/gselements.16.3.179
- Moune, S., Moretti, R., Burtin, A., Jessop, D. E., Didier, T., Robert, V., et al. (2022). Gas monitoring of volcanic-hydrothermal plumes in a tropical environment: The case of La Soufrière de Guadeloupe unrest volcano (Lesser Antilles). *Front. Earth Sci.* 10, 17. doi:10.3389/feart.2022.795760
- Moune, S., Sigmarsson, O., Thordarson, T., and Gauthier, P. J. (2007). Recent volatile evolution in the magmatic system of Hekla volcano, Iceland. *Earth Planet. Sci. Lett.* 255 (3–4), 373–389. doi:10.1016/j.epsl.2006.12.024
- Moussallam, Y., Edmonds, M., Scaillet, B., Peters, N., Gennaro, E., Sides, I., et al. (2016). The impact of degassing on the oxidation state of basaltic magmas: A case study of kilauea volcano. *Earth Planet. Sci. Lett.* 450, 317–325. doi:10.1016/j.epsl.2016.06.031
- Moussallam, Y., Oppenheimer, C., Scaillet, B., Gaillard, F., Kyle, P., Peters, N., et al. (2014). Tracking the changing oxidation state of Erebus magmas, from mantle to surface, driven by magma ascent and degassing. *Earth Planet. Sci. Lett.* 393, 200–209. doi:10.1016/j.epsl.2014.02.055
- Moussallam, Y., Tamburello, G., Peters, N., Apaza, F., Schipper, C. I., Curtis, A., et al. (2017). Volcanic gas emissions and degassing dynamics at Ubinas and Sabancaya volcanoes; implications for the volatile budget of the central volcanic zone. *J. Volcanol. Geotherm. Res.* 343, 181–191. doi:10.1016/j.jvolgeores.2017.06.027
- Mungall, J. E., Brennan, J. M., Godel, B., Barnes, S. J., and Gaillard, F. (2015). Transport of metals and sulphur in magmas by flotation of sulphide melt on vapour bubbles. *Nat. Geosci.* 8 (3), 216–219. doi:10.1038/ngeo2373
- Newhall, C. G., and Self, S. (1982). The volcanic explosivity index (VEI) an estimate of explosive magnitude for historical volcanism. *J. Geophys. Res. Oceans* 87 (C2), 1231–1238. doi:10.1029/jc087ic02p01231
- Oppenheimer, C., Scaillet, B., and Martin, R. S. (2011). Sulfur degassing from volcanoes: Source conditions, surveillance, plume chemistry and Earth system impacts. *Rev. Mineralogy Geochem.* 73 (1), 363–421. doi:10.2138/rmg.2011.73.13
- Oppenheimer, J., Rust, A. C., Cashman, K. V., and Sandnes, B. (2015). Gas migration regimes and outgassing in particle-rich suspensions. *Front. Phys.* 3, 60. doi:10.3389/fphy.2015.00060
- Ottonello, G., Moretti, R., Marini, L., and Zuccolini, M. V. (2001). Oxidation state of iron in silicate glasses and melts: A thermochemical model. *Chem. Geol.* 174 (1–3), 157–179. doi:10.1016/s0009-2541(00)00314-4
- OVSG-IPGP (1999). 2022 Monthly reports on the activity of La Soufrière de Guadeloupe and on regional seismicity. Available at: <http://www.ipgp.fr/fr/ovsg/bulletins-mensuels-de-lovsg>.
- Papale, P., Moretti, R., and Barbato, D. (2006). The compositional dependence of the saturation surface of H<sub>2</sub>O + CO<sub>2</sub> fluids in silicate melts. *Chem. Geol.* 229 (1–3), 78–95. doi:10.1016/j.chemgeo.2006.01.013
- Papale, P., Moretti, R., and Paonita, A. (2022). Thermodynamics of multi-component gas–melt equilibrium in magmas: Theory, models, and applications. *Rev. Mineralogy Geochem.* 87 (1), 431–556. doi:10.2138/rmg.2022.87.10
- Pichavant, M., Poussineau, S., Lesne, P., Solaro, C., and Bourdier, J. L. (2018). Experimental parametrization of magma mixing: Application to the AD 1530 eruption of La soufrière, Guadeloupe (Lesser Antilles). *J. Petrology* 59 (2), 257–282. doi:10.1093/ptrology/egy030
- Pino, N. A., Moretti, R., Allard, P., and Boschi, E. (2011). Seismic precursors of a basaltic paroxysmal explosion track deep gas accumulation and slug upraise. *J. Geophys. Res. Solid Earth* 116 (B2), B02312. doi:10.1029/2009jb000826
- Portnyagin, M., Almeev, R., Matveev, S., and Holtz, F. (2008). Experimental evidence for rapid water exchange between melt inclusions in olivine and host magma. *Earth Planet. Sci. Lett.* 272 (3–4), 541–552. doi:10.1016/j.epsl.2008.05.020
- Poussineau, S. (2005). “Dynamique des magmas andésitiques: Approche expérimentale et pétrostructurale; application à La Soufrière de Guadeloupe et à la Montagne Pelée.” Doctoral dissertation (Orléans, France: Université d’Orléans).
- Putirka, K. D. (2008). Thermometers and barometers for volcanic systems. *Rev. Mineral. Geochem.* 69 (1), 61–120.
- Read, W. G., Froidevaux, L., and Waters, J. W. (1993). Microwave limb sounder measurement of stratospheric SO<sub>2</sub> from the Mt. Pinatubo Volcano. *Geophys. Res. Lett.* 20 (12), 1299–1302. doi:10.1029/93gl00831
- Reed, M. H. (1997). “Hydrothermal alteration and its relationship to ore fluid composition,” in *Geochemistry of hydrothermal ore deposits*. Editor H. L. Barnes 3rd (New York, NY: Wiley), 517–611.
- Robock, A. (2000). Volcanic eruptions and climate. *Rev. Geophys.* 38 (2), 191–219. doi:10.1029/1998rg000054
- Roggensack, K., Hervig, R. L., McKnight, S. B., and Williams, S. N. (1997). Explosive basaltic volcanism from Cerro Negro volcano: Influence of volatiles on eruptive style. *Science* 277 (5332), 1639–1642. doi:10.1126/science.277.5332.1639
- Rosas-Carbajal, M., Komorowski, J. C., Nicollin, F., and Gibert, D. (2016). Volcano electrical tomography unveils edifice collapse hazard linked to hydrothermal system structure and dynamics. *Sci. Rep.* 6 (1), 29899.
- Rose-Koga, E. F., Bouvier, A. S., Gaetani, G. A., Wallace, P. J., Allison, C. M., Andrys, J. A., et al. (2021). Silicate melt inclusions in the new millennium: A review of recommended practices for preparation, analysis, and data presentation. *Chem. Geol.* 570, 120145. doi:10.1016/j.chemgeo.2021.120145
- Rosencrantz, E., and Sclater, J. G. (1986). Depth and age in the Cayman Trough. *Earth Planet. Sci. Lett.* 79 (1–2), 133–144. doi:10.1016/0012-821x(86)90046-4
- Samper, A., Quidelleur, X., Lahitte, P., and Mollex, D. (2007). Timing of effusive volcanism and collapse events within an oceanic arc island: Basse-Terre, Guadeloupe archipelago (Lesser Antilles Arc). *Earth Planet. Sci. Lett.* 258 (1–2), 175–191. doi:10.1016/j.epsl.2007.03.030
- Santer, B. D., Bonfils, C., Painter, J. F., Zelinka, M. D., Mears, C., Solomon, S., et al. (2014). Volcanic contribution to decadal changes in tropospheric temperature. *Nat. Geosci.* 7 (3), 185–189. doi:10.1038/ngeo2098
- Santer, B. D., Solomon, S., Bonfils, C., Zelinka, M. D., Painter, J. F., Beltran, F., et al. (2015). Observed multivariable signals of late 20th and early 21st century volcanic activity. *Geophys. Res. Lett.* 42 (2), 500–509. doi:10.1002/2014gl062366
- Scaillet, B., Clemente, B., Evans, B. W., and Pichavant, M. (1998). Redox control of sulfur degassing in silicic magmas. *J. Geophys. Res. Solid Earth* 103 (B10), 23937–23949. doi:10.1029/98jb02301
- Scaillet, B., Luhr, J., and Carroll, M. R. (2003). Petrological and volcanological constraints on volcanic sulfur emissions to the atmosphere. *Geophys. Monograph-American Geophys. Union* 139, 11–40.
- Scaillet, B., Morizet, Y., Paris, M., and Gaillard, F. (2012). The role of CO<sub>2</sub> on silica undersaturated melt structure: Implication for melt physical properties. *AGU Fall Meet. Abstr.* 2012, MR11C–2508.
- Scaillet, B., and Pichavant, M. (2003). Experimental constraints on volatile abundances in arc magmas and their implications for degassing processes. *Geol. Soc. Lond. Spec. Publ.* 213 (1), 23–52. doi:10.1144/gsl.sp.2003.213.01.03
- Schmidt, A., and Black, B. A. (2022). Reckoning with the rocky relationship between eruption size and climate response: Toward a Volcano–Climate index. *Annu. Rev. Earth Planet. Sci.* 50, 627–661. doi:10.1146/annurev-earth-080921-052816
- Schmidt, A., Mills, M. J., Ghan, S., Gregory, J. M., Allan, R. P., Andrews, T., et al. (2018). Volcanic radiative forcing from 1979 to 2015. *J. Geophys. Res. Atmos.* 123 (22), 12491–12508. doi:10.1029/2018jd028776
- Shaw, A. M., Hauri, E. H., Fischer, T. P., Hilton, D. R., and Kelley, K. A. (2008). Hydrogen isotopes in Mariana arc melt inclusions: Implications for subduction dehydration and the deep-Earth water cycle. *Earth Planet. Sci. Lett.* 275 (1–2), 138–145. doi:10.1016/j.epsl.2008.08.015
- Sisson, T. W., and Grove, T. L. (1993). Experimental investigations of the role of H<sub>2</sub>O in calc-alkaline differentiation and subduction zone magmatism. *Contributions mineralogy petrology* 113 (2), 143–166. doi:10.1007/bf00283225
- Solomon, S., Daniel, J. S., Neely, R. R., Vernier, J. P., Dutton, E. G., and Thomason, L. W. (2011). The persistently variable “background” stratospheric aerosol layer and global climate change. *Science* 333 (6044), 866–870. doi:10.1126/science.1206027
- Solomon, S., Ivy, D. J., Kinnison, D., Mills, M. J., Neely, R. R., III, and Schmidt, A. (2016). Emergence of healing in the Antarctic ozone layer. *Science* 353 (6296), 269–274. doi:10.1126/science.aae0061
- Sparks, R. S. J., Bursik, M. I., Carey, S. N., Gilbert, J., Glaze, L. S., Sigurdsson, H., et al. (1997). *Volcanic plumes*. Hoboken, NJ: Wiley.
- Symithe, S., Calais, E., de Chabalière, J. B., Robertson, R., and Higgins, M. (2015). Current block motions and strain accumulation on active faults in the Caribbean. *J. Geophys. Res. Solid Earth* 120, 3748–3774. doi:10.1002/2014JB011779
- Symonds, R. B., Gerlach, T. M., and Reed, M. H. (2001). Magmatic gas scrubbing: Implications for volcano monitoring. *J. Volcanol. Geotherm. Res.* 108 (1–4), 303–341. doi:10.1016/s0377-0273(00)00292-4
- Tait, S., Jaupart, C., and Vergnolle, S. (1989). Pressure, gas content and eruption periodicity of a shallow, crystallising magma chamber. *Earth Planet. Sci. Lett.* 92 (1), 107–123. doi:10.1016/0012-821x(89)90025-3
- Tamburello, G., Moune, S., Allard, P., Venugopal, S., Robert, V., Rosas-Carbajal, M., et al. (2019). Spatio-temporal relationships between fumarolic activity, hydrothermal fluid circulation and geophysical signals at an arc volcano in degassing unrest: La Soufrière de Guadeloupe (French West Indies). *Geosciences* 9 (11), 480. doi:10.3390/geosciences9110480
- Textor, C., Graf, H. F., Herzog, M., and Oberhuber, J. M. (2003). Injection of gases into the stratosphere by explosive volcanic eruptions. *J. Geophys. Res. Atmos.* 108 (D19), 4606. doi:10.1029/2002jd002987
- Thomason, L. W., Kovilakam, M., Schmidt, A., Von Savigny, C., Knepp, T., and Rieger, L. (2021). Evidence for the predictability of changes in the stratospheric aerosol size following volcanic eruptions of diverse magnitudes using space-based instruments. *Atmos. Chem. Phys.* 21 (2), 1143–1158. doi:10.5194/acp-21-1143-2021

- Timmreck, C. (2012). Modeling the climatic effects of large explosive volcanic eruptions. *Wiley Interdiscip. Rev. Clim. Change* 3 (6), 545–564. doi:10.1002/wcc.192
- Todd, C. S. (1996). Fluorine analysis by electron microprobe: Correction for iron interference. *Geol. Soc. Am. Abstr.* 28 (7), 212.
- Van Donk, J. (1976). *O18 record of the atlantic ocean for the entire pleistocene epoch*. doi:10.1130/MEM145-p147
- Venugopal, S., Schiavi, F., Moune, S., Bolfan-Casanova, N., Druitt, T., and Williams-Jones, G. (2020). Melt inclusion vapour bubbles: The hidden reservoir for major and volatile elements. *Sci. Rep.* 10 (1), 9034–9114. doi:10.1038/s41598-020-65226-3
- Villemant, B., Komorowski, J. C., Dessert, C., Michel, A., Crispi, O., Hammouya, G., et al. (2014). Evidence for a new shallow magma intrusion at La soufrière of Guadeloupe (lesser Antilles): Insights from long-term geochemical monitoring of halogen-rich hydrothermal fluids. *J. Volcanol. Geotherm. Res.* 285, 247–277. doi:10.1016/j.jvolgeores.2014.08.002
- Wallace, P. J. (2003). “From mantle to atmosphere: Magma degassing, explosive eruptions, and volcanic volatile budgets,” in *Developments in volcanology*, 5, 105–127. doi:10.1016/S1871-644X(03)80026-8
- Wallace, P. J., and Gerlach, T. M. (1994). Magmatic vapor source for sulfur dioxide released during volcanic eruptions: Evidence from Mount Pinatubo. *Science* 265 (5171), 497–499. doi:10.1126/science.265.5171.497
- Wallace, P. J. (2005). Volatiles in subduction zone magmas: Concentrations and fluxes based on melt inclusion and volcanic gas data. *J. Volcanol. Geotherm. Res.* 140 (1–3), 217–240. doi:10.1016/j.jvolgeores.2004.07.023
- Wallace, P. J. (2001). Volcanic SO<sub>2</sub> emissions and the abundance and distribution of exsolved gas in magma bodies. *J. Volcanol. Geotherm. Res.* 108 (1–4), 85–106. doi:10.1016/S0377-0273(00)00279-1
- Williams, S. N., Sturchio, N. C., Mendez, R., Londoño, A., García, N., and García P., N. (1990). Sulfur dioxide from nevado del Ruiz volcano, Colombia: Total flux and isotopic constraints on its origin. *J. Volcanol. Geotherm. Res.* 42 (1–2), 53–68. doi:10.1016/0377-0273(90)90069-r
- Wilson, L. R., Sparks, S. J., and Walker, G. P. L. (1980). Explosive volcanic eruptions—IV. The control of magma properties and conduit geometry on eruption column behaviour. *Geophys. J. International* 63 1, 117–148. doi:10.1111/j.1365-246X.1980.tb02613.x
- Witter, J. B., and Kuehner, S. M. (2004). A simple empirical method for high-quality electron microprobe analysis of fluorine at trace levels in Fe-bearing minerals and glasses. *Am. Mineralogist* 89 (1), 57–63. doi:10.2138/am-2004-0108
- Yao, Z., and Mungall, J. E. (2020). Flotation mechanism of sulphide melt on vapour bubbles in partially molten magmatic systems. *Earth Planet. Sci. Lett.* 542, 116298. doi:10.1016/j.epsl.2020.116298
- Zlotnicki, J., Feuillard, M., and Hammouya, G. (1994). Water circulations on La Soufrière volcano inferred by self-potential surveys (Guadeloupe, Lesser Antilles). Renew of volcanic activity? *J. geomagnetism Geoelectr.* 46 (9), 797–813. doi:10.5636/jgg.46.797
- Zurek, J., Moune, S., Williams-Jones, G., Vigouroux, N., and Gauthier, P. J. (2019). Melt inclusion evidence for long term steady-state volcanism at Las Sierras-Masaya volcano, Nicaragua. *J. Volcanol. Geotherm. Res.* 378, 16–28. doi:10.1016/j.jvolgeores.2019.04.007